



Paleoceanography and Paleoclimatology^{*}

RESEARCH ARTICLE

10.1029/2024PA004995

Key Points:

- Indian Summer Monsoon runoff and marine productivity reconstructions from the Bay of Bengal in the Late Pliocene-Early Pleistocene
- Nuanced responses to eccentricity, obliquity, and precession change in dominance in step with global and regional climate patterns
- High CO₂, low ice volume intervals provide insights into potential future monsoon dynamics and their response to external forcing factors

Supporting Information:

Supporting Information may be found in the online version of this article.

Correspondence to:

Y. Bokhari-Friberg and P. Anand, ybokfri@gmail.com; pallavi.anand@open.ac.uk

Citation:

Bokhari-Friberg, Y., Anand, P., Romero, O., Littler, K., Robinson, M., Sexton, P., et al. (2025). Influence of Indian Summer Monsoon on marine biological productivity across the Late Pliocene and Early Pleistocene. *Paleoceanography and Paleoclimatology*, 40, e2024PA004995. https://doi.org/10.1029/2024PA004995

Received 18 AUG 2024 Accepted 27 MAR 2025

© 2025. The Author(s). This is an open access article under the terms of the Creative Commons Attribution License, which permits use, distribution and reproduction in any medium, provided the original work is properly cited.

Influence of Indian Summer Monsoon on Marine Biological Productivity Across the Late Pliocene and Early Pleistocene

Yasmin Bokhari-Friberg^{1,2} , Pallavi Anand¹ , Oscar Romero³ , Kate Littler⁴, Marci Robinson⁵ , Philip Sexton¹, Melanie Leng⁶ , and Masafumi Murayama^{7,8}

¹School of Environment, Earth and Ecosystem Sciences, The Open University, Milton Keynes, UK, ²School of Natural Sciences, Macquarie University, Sydney, NSW, Australia, ³MARUM, Centre for Marine Environmental Sciences, University of Bremen, Bremen, Germany, ⁴Camborne School of Mines, Earth and Environmental Sciences Department, & Environment and Sustainability Institute, University of Exeter, Penryn, UK, ⁵U.S. Geological Survey, Florence Bascom Geoscience Center, Reston, VA, USA, ⁶National Environmental Isotope Facility, British Geological Survey, Nottingham, UK, ⁷Faculty of Agriculture and Marine Science, Kochi University, Kochi, Japan, ⁸Center for Advanced Marine Core Research, Kochi University, Kochi, Japan

Abstract The Indian Summer Monsoon (ISM) significantly impacts the lives of billions of people through rainfall patterns and ocean biological productivity. However, its stability both in the near future and distant past is disputed, particularly its response to changing temperatures and global ice volume. Here, we present a comprehensive multiproxy reconstruction of ISM-induced runoff and marine biological productivity from the Late Pliocene to the Early Pleistocene (3.5–2.3 Ma), using high-resolution deep-sea sediment records from the northern Bay of Bengal (BoB). This critical interval is characterized by high but falling atmospheric CO₂ levels and the establishment of Northern Hemisphere glaciation, but with a similar paleogeography to the modern. Our orbitally-tuned records, based on bulk sediment X-Ray fluorescence-elemental data and diatom and planktic foraminiferal assemblages, reveal that periods of diminished marine biological productivity coincide with elevated ISM runoff, reflecting the interplay between freshwater input, turbidity, and nutrient availability off northeastern India. Moreover, our analysis highlights the sensitivity of the ISM strength and BoB ecosystem to orbital forcing. We observe the presence of eccentricity, obliquity, and precession cyclicities in the runoff and productivity records, with multiple transitions in the dominant orbital frequency during the study interval, pointing to unique sensitivities of ISM rainfall/runoff to Earth's orbital forcing. These findings underscore the importance of considering both orbital forcing and internal climate dynamics in understanding ISM variability and its implications for marine ecosystems.

Plain Language Summary The Indian Summer Monsoon (ISM) is a vital weather system that brings significant rainfall to South Asia each summer, affecting billions of people through rain patterns and ocean health, but it is vulnerable to disruption due to anthropogenic climate change. This study investigates ISM runoff and marine biological productivity in the northwestern Bay of Bengal (BoB) from 3.5 to 2.3 million years ago. During this period, Earth experienced major changes with falling atmospheric CO2 concentrations, increasing global ice volume, and falling sea level. By examining marine sediments from the BoB, we found that stronger ISM rainfall led to increased freshwater runoff into the ocean, which reduced marine biological productivity. This is because increased runoff brings more sediments into the ocean, increasing turbidity and limiting light required for phytoplankton in the surface, while also forming a freshwater surface layer that reduces the amount of nutrients upwelling from deeper waters. We found that these changes in ISM strength and marine productivity were influenced by Earth's orbital cycles, which varied in relative importance with time. These findings highlight how closely linked the ISM is to both global climate changes and local marine ecosystems, helping us better understand potential future monsoon behavior.

1. Introduction

The Indian Summer Monsoon (ISM) is a critical component of the global climate system, providing vital rainfall for the agricultural and water resources of the Indian subcontinent, which hosts a fifth of the world's population (Menon et al., 2013; Turner & Annamalai, 2012). ISM dynamics are defined by two components: thermodynamic (rainfall) and dynamic (wind). ISM wind drives coastal upwelling in the Arabian Sea and along the Indian margins that supports delicate marine ecosystems and the livelihoods of those who rely on them, and also controls

the carbon storage potential of these waters (Sarma et al., 2020). Present day seasonal ISM continental rainfall and resultant freshwater input via runoff suppress marine biological productivity in the northern Bay of Bengal (BoB). The freshwater input following ISM runoff creates a freshwater surface layer inhibiting upwelling. Additionally, large scale cloud cover and/or input of continental materials causes turbidity in the surface layer, affecting sunlight availability, which impedes phytoplankton growth (Jyothibabu et al., 2018). The future changes in ISM rainfall/runoff in this region is therefore of major societal importance (Chen et al., 2020; Ha et al., 2020; Wang et al., 2020). Relative changes in ISM wind and rainfall and their relationships could affect marine productivity under different climate settings in response to a range of external and internal forcing factors, including orbital variations and ocean-atmosphere interactions.

Climate models predict that greenhouse gas-induced warming will strengthen the ISM (rainfall), due to a strong thermodynamic sensitivity in the models, increasing the moisture content of air masses and the likelihood of extreme events (Annamalai, 2007). In contrast, the monsoon winds are predicted to weaken due to Indian Ocean warming following a reduced ocean-land temperature gradient (Pörtner et al., 2019). Yet this apparent future decoupling of the dynamic and thermodynamic components of the monsoon has not been observed in past records. Previous ISM reconstructions beyond the Late Pleistocene have mainly come from the Arabian Sea, reflecting wind strength (Bloemendal & DeMenocal, 1989; Clemens et al., 1996, 2008) rather than rainfall. Additionally, the effect of changing ISM rainfall/runoff on marine biological productivity in the region and its relationship with external and internal drivers are unknown. To address these gaps in our knowledge, we present reconstructions of coupled continental rainfall/runoff and marine biological productivity during the Late Pliocene and earliest part of the Early Pleistocene (3.5–2.3 Ma) when global boundary conditions were evolving, for example, average global temperatures and atmospheric CO₂ levels were similar to, or exceeded, those of the early 21st century.

The target period of the Late Pliocene–Early Pleistocene (3.5–2.3 Ma) is one of great climatic upheavals, but with similar paleogeographies to the modern world, and hence, may be a useful analog for the near future (Haywood et al., 2016; Westerhold et al., 2020). Following a period of relatively warm and stable conditions, the intensification of Northern Hemisphere Glaciation (iNHG) began in the Late Pliocene ~3.2-3.0 Ma. This glaciation initially started in the Southern Ocean and Antarctic region, before the signal propagated to the Northern Hemisphere (NH) mid- and high latitudes, coinciding with a great expansion of NH ice sheets around 2.7 Ma (McClymont et al., 2023). Atmospheric CO₂ levels also dropped from ~300 to 400 ppm to 250–350 ppm at ~2.8 Ma, which may have acted as a trigger for global cooling (De la Vega et al., 2020; Martínez-Botí et al., 2015). Several published low-latitude palaeoceanographic records, including those from monsoonal regions, show a change in orbital frequency in the latest Pliocene broadly coincident with iNHG (Bloemendal & DeMenocal, 1989; Cai et al., 2018; Clemens et al., 1996; Gupta et al., 2015; Gupta & Thomas, 2003; Huang et al., 2007; Singh, 2021). These low-latitude precession-paced monsoon wind records exhibit an increase in obliquity dominance around 2.8-2.7 Ma, which has been attributed to teleconnections between the growing high latitude ice sheets and the low latitude monsoon systems (Geirsdottir & Eiriksson, 1994; Raymo, 1994). However, we did not have complementary records from the core Indian Monsoon region (e.g., the BoB) for the interval 3.5– 2.4 Ma with which to test if these patterns are applicable across the breadth of the low latitudes, including the Indian Monsoon rainfall system. Therefore, well-constrained, high-resolution runoff and productivity proxy records from the BoB are required to test whether ISM runoff displays similar orbital switches in the Late Pliocene, and if so, what this may imply for the sensitivity of the ISM system to external drivers. Identifying past relationships between orbital parameters and ISM dynamics can help refine climate models and projections, enhancing our ability to predict future changes in monsoon behavior.

X-ray fluorescence (XRF)-derived elemental ratios have been proven to be useful proxies for capturing continental rainfall/runoff as well as productivity. K, Al, and Rb are used as a proxy for fine-grained terrigenous sediments as they are present in clay minerals, while Ti and Zr represent coarse-grained sediment (Banerji et al., 2022; Clift et al., 2008; Piva et al., 2008; Rothwell & Rack, 2006; Wei et al., 2006). Elements such as Ca and Si have their origin from both marine biogenic carbonate and siliceous microfossils as well as post depositional sources during the formation of gypsum/anhydrite for Ca and Si from terrigenous input (runoff), respectively. All terrestrially-derived crustal elements (i.e., elements transported from the continent) are expected to increase during higher continental seasonal monsoon runoff. Therefore, an ISM runoff stack was created including the sum of the elements K, Al, Rb, Ti, and Zr and normalizing it to all element counts. XRF counts of the aforementioned elements have previously been used as indicators of runoff, minerogenic input, and/or detrital input (Gebregiorgis

BOKHARI-FRIBERG ET AL. 2 of 18

25724525, 2025, 7, Downloaded from https://agupubs.onlinelibrary.wiley.com/doi/10.1029/2024PA004995 by British Geological Survey, Wiley Online Library on [03/10/2025]. See

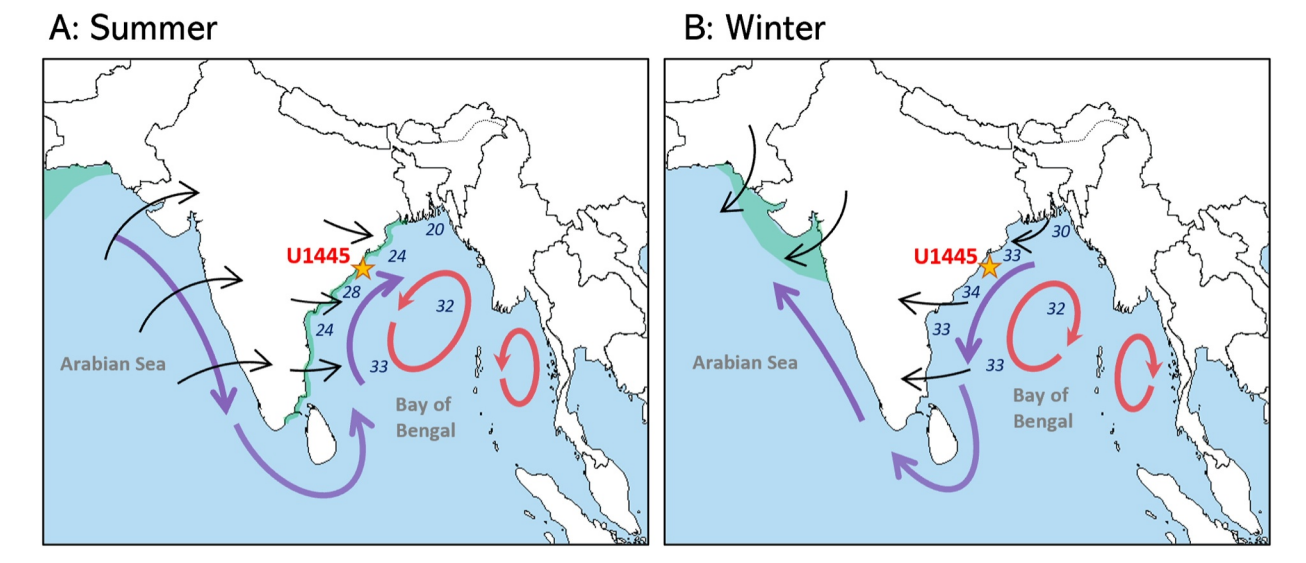


Figure 1. The Bay of Bengal in the present day with ocean currents (colored arrows) and marine productivity (green) in summer (a) and winter (b). Black arrows represent the dominant seasonal wind direction and numbers denote salinity at the end of summer (a) and winter (b), respectively. International Ocean Discovery Program Site U1445 is marked with a star.

et al., 2020; Kylander et al., 2011; Wilson et al., 2018). While Fe is often used as a terrigenous element, it was excluded from this stack due to its origin from both continental and post-depositional (e.g., pyrite) sources. Additionally, Fe exhibits high abundance in the sediment (~84% of all counts), which masks the variability of less abundant but more diagnostic terrigenous elements in the composite data sets. See Figures S1 and S2 in Supporting Information S1 for detailed XRF cross-plots and raw data plots.

In studies of hemipelagic sediment (e.g., from the Arabian Sea and Japan Sea), Br has been shown to be positively correlated with total organic carbon content of the sediment and used as a primary productivity proxy in both marine and lacustrine environments (Gilfedder et al., 2011; Seki et al., 2019; Ziegler et al., 2008). As such, it has become established as a valuable paleoproductivity indicator in both marine and lacustrine environments. At Site U1445 the organic-bound Br could be derived either from the continental source or from the marine primary productivity, associated either with siliceous (e.g., diatoms) or calcareous (e.g., coccolithophores) organisms. Additionally, the abundance and distribution of marine diatoms (siliceous microscopic algae) within hemipelagic sediments are important indicators of past climate and ocean conditions in the BoB. They provide information about changes in ocean temperature, salinity, and nutrient availability over time.

This study uses high-resolution runoff (\sim 100 years) and productivity (\sim 3 kyr) records from the northwestern BoB to examine the relationship between ISM rainfall, marine biological productivity, orbital parameters, and high-latitude climate in the Late Pliocene and earliest Pleistocene. Analyses of these records provide insights into past monsoon dynamics and their implications for future climatic changes.

2. Materials and Methods

2.1. Study Area and Sample Collection

We used marine sediments recovered from International Ocean Discovery Program (IODP) Site U1445 in the southern end of the Mahanadi Basin (northwestern BoB), which receives freshwater input from the combined Ganges-Brahmaputra-Meghna-Mahanadi river system (Figure 1). The site is situated 94 km offshore NE India (17°N, 84°E) and has a modern water depth of 2,513 mbsl (meters below sea level). Late Pliocene sediments are mainly hemipelagic clays with a large biogenic fraction, including foraminifera, diatoms, and nannofossils (Clemens et al., 2016). The BoB contains the world's largest submarine fan, the Bengal Fan, which covers an area of ~3 million km², but does not extend over the Mahanadi Basin (Curray et al., 2002). Today the bay receives about 1.7 billion tons of sediments per year (Kuehl et al., 1989; Milliman & Meade, 1983), much of it as a result of ISM runoff. The proximal location of Site U1445 ideally captures freshwater flux and sediment deposition

BOKHARI-FRIBERG ET AL. 3 of 18



10.1029/2024PA004995

resulting from ISM continental rainfall and river runoff, but in a lithology (e.g., hemipelagic clay with microfossils) that is amenable to multi-proxy paleoceanographic reconstruction. Work on Late Pleistocene sediments from the Mahanadi Basin, including the nearby sister site IODP U1446, has already yielded important insights into geologically more recent ISM behavior (Clemens et al., 2021; Nilsson-Kerr et al., 2022; Yamamoto et al., 2022), but Pliocene ISM dynamics remain unconstrained.

This study uses sediments from Holes A and C drilled at Site U1445. Hole A was drilled using the advanced piston corer (APC) system to 225.1 m depth below seafloor (DBS) (Core 353-U1445A-24H), after which the extended core barrel (XCB) system was deployed (from Core 353-U1445A-25X). Hole C was drilled using the APC system to 218.2 m DBS (353-U1445C-24H), after which the XCB system was deployed (from Core 353-U1445C-25X). Hole A was drilled to a total depth of 672.6 m DBS, while Hole C was drilled to a total depth of 305.2 m DBS (Clemens et al., 2016).

2.2. Stratigraphic Splice and Geochronology for Site U1445

The Site U1445 record used herein constitutes a stratigraphic splice amalgamating data from Holes A and C, correlated on the basis of XRF elemental abundance data and elemental ratios, and further modified using benthic foraminifera oxygen isotope (δ^{18} O) data (see Section S1 and Tables S1 and S2 in Supporting Information S1 for details).

An accurate chronology is essential for putting rainfall and productivity changes captured in BoB sediments into temporal context and for making meaningful comparisons with records from other regions, as well as for identifying the timing of monsoon intensification and the associated effects on ocean productivity and sedimentation patterns with respect to orbital parameters. An orbital-scale age model for Site U1445 was constructed using benthic foraminiferal (Uvigerina spp. and Cibicidoides wuellestorfi) stable oxygen isotopes ($\delta^{18}O$) (see Section S2, Figures S3 and S4, and Table S3 in Supporting Information S1 for details).

2.3. XRF Scanning for Bulk Element Composition

XRF scanning provides bulk sediment elemental data that are commonly utilized for reconstructing past climate and ocean conditions in marine sediments (Löwemark et al., 2019; Rothwell & Croudace, 2015). XRF data can provide important information about the source and depositional history of the sediments, to infer past climate and ocean conditions. The sample is bombarded with high energy X-rays, which excites electrons, leading to the emission of fluorescent X-rays absorbed by a detector. Sediment core sections from Site U1445 were XRF scanned at 1 or 2 cm resolution using a Cox Analytical ITRAX Core Scanner at Kochi University, Japan. Sections were kept in a cold storage and scanned with a Mo (molybdenum) tube set at 30 kV and 55 mA with XRF time of 15 s. The X-ray beam size ("footprint") was 0.2 mm by 20 mm and the XRF detector window size was 2 mm by 8 mm. Sections were prepared for scanning by cleaning the surface layer to reveal a fresh, flat, and even surface. They were then placed in the ITRAX with a thin XRF polypropylene film laced over the section. The abundance of 49 different elements was determined during scanning: Al, Si, P, S, Cl, Ar, K, Ca, Sc, Ti, V, Cr, Mn, Fe, Co, Ni, Cu, Zn, Ga, Ge, As, Se, Br, Rb, Sr, Y, Zr, Ag, Cd, Sn, Sb, Cs, Ba, La, Ce, Pr, Nd, Eu, Tb, Dy, Yb, Hf, Ta, W, Pt, Pb, Th, Pa, U.

2.4. Diatom Counts

Diatom species were identified and counted on permanent slides (Mountex mounting medium). Several traverses across each slide were systematically tracked to obtain a representative count of valves (450–800 valves per slide). A Zeiss Axioscop with interference illumination (MARUM, University of Bremen) was used for the analysis of \sim 530 samples. The counting of two replicate slides at x1000 magnification indicates an analytical error of 10.0%. Sediments were freeze-dried and prepared using the acid-based method, and the census procedure and the definition of counting units followed standard protocols outlined by Schrader and Gersonde (1978). The resulting counts yielded concentration of valves or bodies per g^{-2} (marine diatom concentration), calculated as follows:

concentration = [N] x [A/a] x [1/W] x [V/v]

BOKHARI-FRIBERG ET AL. 4 of 18



10.1029/2024PA004995

where, [N] is the number of valves in a known area [a], as a fraction of the total area of a petri dish [A], the sample weight [W] in g, and the final sample volume (V) and sample volume used for the permanent slide (v) (Sancetta & Calvert, 1988).

2.5. Planktic Foraminiferal Species Assemblages

One hundred and sixty-seven samples between 3.3 and 2.7 Ma were analyzed for planktic foraminiferal assemblage data, with a resolution of 3.8 kyrs. In this study, we focus on the percent abundance of the upwelling indicator species *Globigerina bulloides*. This species is widely recognized as a valuable proxy for past oceanic conditions, particularly upwelling events (Kroon et al., 1991). Its abundance in sedimentary records provides insights into historical changes in water column stratification, nutrient availability, and sea surface temperatures (Shrivastav et al., 2016). Samples of ~17 cm³ were collected at a sampling resolution of ~40 cm from U1445 A core material. Samples were freeze-dried then placed on an orbital shaker for ~1 hr in a sodium hexameta-phosphate solution for sediment disaggregation. Samples were then washed through a 63 µm sieve to remove the mud fraction and oven dried at ~45°C. A split of ~300 specimens was collected from the >150 µm size fraction of most samples; in samples where specimens were less abundant, all foraminifers were collected. Samples were examined under a light microscope to determine preservation, and planktonic foraminifera species were transferred to a micropaleontologic slide where they were identified to the species level and counted. Sample slides and residues are archived in the PRISM lab at the U.S. Geological Survey National Center in Reston, Virginia, USA. The census data are archived with ScienceBase.gov and can be found by accessing this link: https://www.sciencebase.gov/catalog/item/64f76f5cd34ed30c20544b7d (Robinson & Dowsett, 2023).

2.6. Spectral Analysis

Spectral, frequency, and phase analysis of climate proxies enable the identification of patterns and relationships in climate data and provide valuable information about the mechanisms of past changes. Spectral and frequency analysis are used to determine the most common dominant frequency and to identify any periodicities or cyclical patterns in the data. Phase analysis can provide information about the timing (leads and lags) of the relationships, and can be used to determine the causes and mechanisms of past climate changes and to understand the feedbacks between different climate variables.

In this study, evolutionary spectral analysis, multi-taper method (MTM) analysis, and phase and coherency analyses were performed in Analyseries (Paillard et al., 1996) and Acycle (M. Li et al., 2019) software. Cross-spectra were calculated in terms of obliquity or precession (Laskar, 2004), where minimum precession is defined by 90°N 21st June (standard definition: ϖ is from vernal point, param = e sin (ϖ)). BTukey cross-spectra was set to a bandwidth of 0.0125, confidence level of 90%, using a Bartlett window. Where phase is expressed as radians, the number is converted to degrees by dividing the number by π and multiplying by 180. Data were detrended to remove long-term cycles on timescales of 200 kyr or longer. The XRF derived high-resolution data from U1445 (normalized Br and runoff stack) are used raw, that is, no moving average is applied when performing coherence and phase analyses, as opposed to when displayed visually with a 9-point moving average. Several smoothings were tested (raw, 3pt, 5pt, 9pt, and 19pt moving average) to compare their coherence and phase relationships with precession. These values were selected to compare a wide variety of smoothings. The raw, 3pt and 5pt moving averages were identical in the relevant frequencies (19 kyr and lower) but started diverging in the higher frequencies (from ~16 kyr and higher). The raw data was deemed more appropriate to avoid losing resolution and biasing the frequencies.

2.7. Phase Relationships

To evaluate the leads and lags between internal and external climate forcing factors and their relationship with ISM rainfall/runoff and wind derived productivity, we use the phase wheel approach. The wheels are displayed as 360° circles where arrows pointing upwards (i.e., ~0°) indicate correlation between proxy and Omax (obliquity maxima) or Pmin (precession minima), and arrows pointing downwards (~180°) indicate anti-correlation. Arrows pointing to the right side of the wheel (i.e., clockwise from Omax/Pmin) indicate lags, and arrows on the left side indicate leads. The full Omax circle represents 41 kyr and the full Pmin circle represents 23 kyr, so that leads/lags in degrees can be converted to leads/lags in kiloyears:

BOKHARI-FRIBERG ET AL. 5 of 18

25724325, 2025, 7, Downloaded from https://agupubs.onlinelibrary.wiley.com/doi/10.1029/2024PA/004995 by British Geological Survey, Wiley Online Library on [03/10/2025]. See the Terms and Conditions

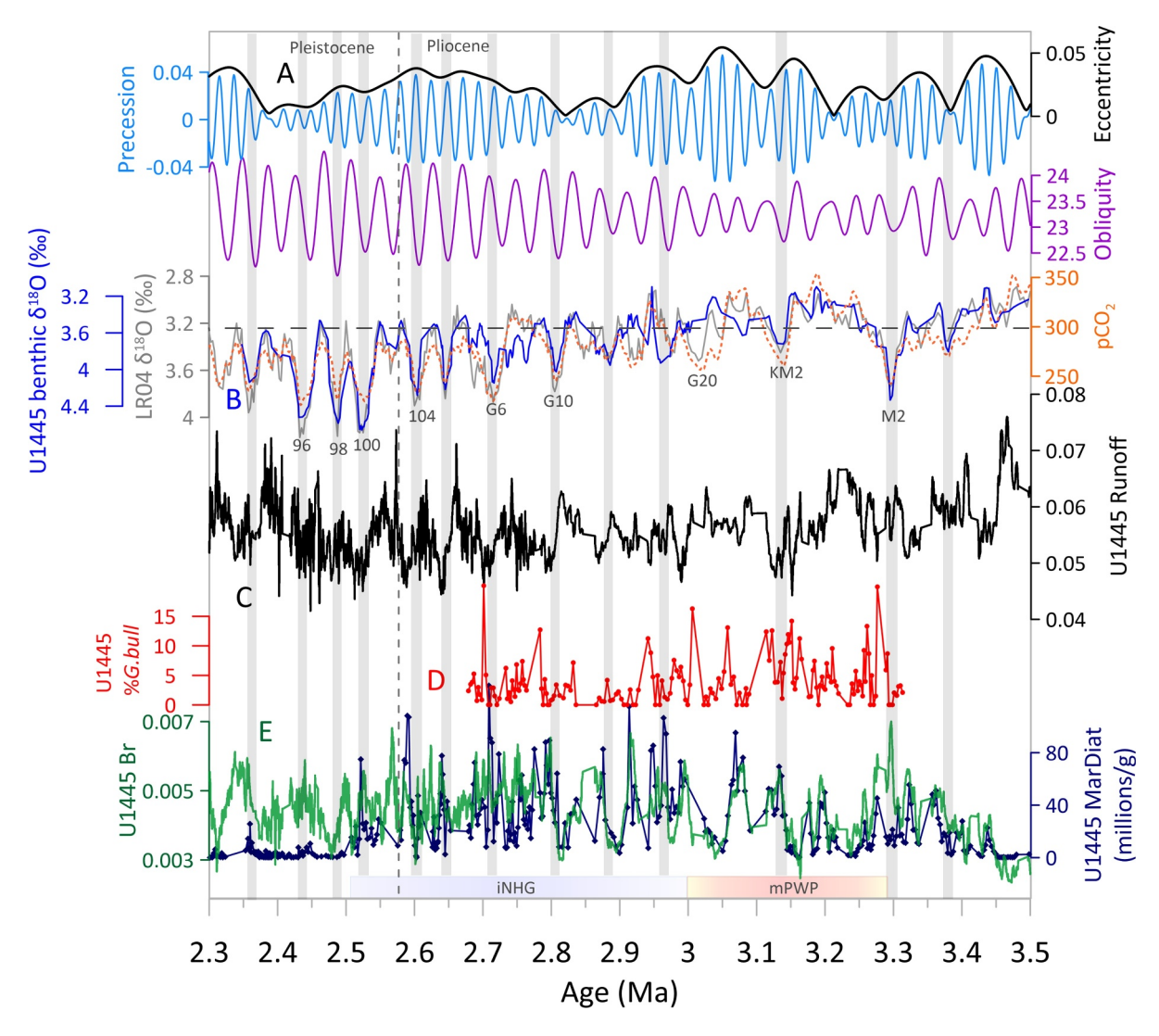


Figure 2. Compilation of Site U1445 records with external forcings in the time window 2.3–3.5 Ma. (a) Eccentricity (black), precession (blue) and obliquity (purple) (Laskar, 2004). (b) LR04 (gray) and U1445 (blue) benthic $\delta^{18}O$ (%_e) with modern value (3.23%_e) as a blue dotted line. Orange: Reconstructed pCO₂ (Berends et al., 2021). (c) U1445 runoff stack (black). (d) U1445% *G. bulloides*, representing upwelling (red). (e) U1445 Br (green) and marine diatom concentration (millions of valves/g) (blue). The mid-Piacenzian warm period and initiation of Northern Hemisphere glaciation (iNHG) are highlighted in red and blue, respectively. See Figure S5 in Supporting Information S1 for a version of this figure with D overlain on (e).

$$\frac{\text{Cycle length (kyr)}}{360^{\circ}} \times \text{Lead or lag (°)} = \text{Lead or lag (kyr)}$$

Only records with a coherency over 0.38 (the limit for non-zero coherence) are plotted. Records with coherence of 0.38–0.50 are plotted with dotted lines, and those with coherence >0.50 are plotted with full lines.

3. Results

3.1. ISM Runoff and Marine Biological Productivity Trends

Figure 2 presents runoff intensity (C) and marine biological productivity (D, E) from Site U1445 in context with changes in Earth's orbit (A), global ice volume and CO_2 (B) from the Late Pliocene (3.5 Ma) to the Early Pleistocene (2.3 Ma). At orbital scales, runoff shows a general relationship with benthic $\delta^{18}O$, where interglacials (more negative $\delta^{18}O$) generally coincide with higher runoff across the study interval (e.g., MIS KM5 (3.23 Ma), G1 (2.62 Ma), 101 (2.55 Ma), 97 (2.46 Ma)), while glacials tend to correspond with lower runoff (e.g., KM2

BOKHARI-FRIBERG ET AL. 6 of 18

(3.14 Ma), G10 (2.8 Ma), G2 (2.64 Ma), 100 (2.53 Ma)) (Figures 2b and 2c). Similarly, the productivity proxies often parallel these trends with peaks during the glacials (e.g., MIS M2 (3.30 Ma), KM2 and G10) and declines during interglacials (e.g., MIS MG5 (3.46 Ma), G1) (Figures 2b–2d and 2e). While this general relationship holds true across much of the study interval, there are exceptions, particularly in the younger intervals, where the correlation between rainfall and productivity becomes less distinct (see Section 4.4 for details).

3.2. ISM Runoff and Marine Biological Productivity Orbital Frequencies

For spectral analysis, we selected the time frame 3.5–2.4 Ma, instead of 3.5–2.3 Ma, due to the increased uncertainty associated with the very end of the age model record (2.3 Ma). The early part of the age model extends beyond 3.5 Ma, ensuring high confidence in the selected timeframe. Spectral analysis of the ISM runoff and productivity data reveals significant power across various orbital frequencies, including eccentricity, obliquity and precession, as well as heterodynes, which represent combinations of these frequencies (Figure 3). Within the entire 3.5–2.4 Ma record, we discern notable variations in the distribution of spectral power across each proxy record, and identify three key intervals in the new ISM data based on this evolutionary spectral analysis (Figure 3). These intervals are divided into the following time windows for MTM analysis: Interval 1: 3.15–3.50 Ma; Interval 2: 2.75–3.15 Ma; and Interval 3: 2.40–2.75 Ma (Figure 4). MTM analysis of the ISM runoff and productivity data reveals significant power across various orbital frequencies, including obliquity and precession. While spectral power is observed at the 100-kyr eccentricity frequency, we acknowledge that time slices shorter than 400 kyr may not provide statistically robust detection of eccentricity cycles (Wunsch, 2004). To reflect this limitation, we have indicated the 100-kyr component with a dotted line in Figure 4, acknowledging its presence but also its lower statistical robustness in short intervals.

In the runoff stack record, Interval 1 features the influence of precession, whereas obliquity is weak. Interval 2 exhibits moderate precession and strengthened obliquity, and the former further weakens in Interval 3. In the Br record, Interval 1 is characterized by a dominant precession signal alongside a subdued obliquity component, similar to runoff. Transitioning into Interval 2, obliquity strengthens while precession weakens, only to resurge in power during Interval 3, which shows both stronger precession and obliquity than the equivalent interval in runoff. In the marine diatom record, obliquity stands out as the dominant orbital frequency during Interval 1. However, a distinctive shift occurs around 3.2 Ma, coinciding with the onset of the mid-Piacenzian warm period (mPWP), leading to the abrupt decline in obliquity's influence. Intervals 2 and 3 exhibit spectral frequencies that closely resemble those observed in the Br data set. It should be noted that the resolution of the marine diatom record is lower than that of Br, making the latter more reliable for spectral analysis in this case.

Eccentricity power and its associated heterodynes also make their presence known across most of the runoff, diatom, and Br records. Intriguingly, obliquity power remains notably weak during a significant portion of the mPWP (late Interval 1). However, it makes a resurgence in all three data sets, largely coinciding with the period around 3.1–3.0 Ma (MIS G20–G21). Visual inspection of the data further reveals an apparent shift in frequency within the runoff data set around 2.8 Ma (MIS G10), characterized by a transition to more "noisy" data (Figure 2). This transition phase is echoed in the productivity proxies, albeit slightly delayed, at around 2.72 Ma (MIS G6).

4. Discussion

4.1. Reliability of Bulk Sediment Br as a Productivity Proxy

Before discussing the implications of the new records in terms of ISM-related runoff and palaeoproductivity, and their relationship to global climate trends, we first discuss the reliability of the proxies. The use of terrigenous elements as a proxy for ISM runoff at the study site has been explained earlier (see Section 2) and has previously been applied in the BoB (Nilsson-Kerr et al., 2022; Phillips et al., 2014). However, Br as a productivity proxy has not yet been tested in BoB sediments, although it has been previously used in several studies in the Japan Sea and Arabian Sea (Seki et al., 2019; Ziegler et al., 2008). To establish the reliability of XRF-derived Br abundance as a productivity proxy at Site U1445, Br data was compared with an independent measure of marine productivity from the same samples—marine diatom concentration (Figure 2e) (Bradtmiller et al., 2006; Werner & Roth, 1977). The visual coherence between the two records underscores the reliability of Br as a (siliceous) productivity indicator at Site U1445 for most of the study interval (3.5–2.5 Ma). Moreover, the generally inverse relationship between Br and the runoff stack (Figures S8 and S9 in Supporting Information S1) suggests that Br is not principally derived from terrestrial organic matter introduced via runoff. Instead, it likely originates from a

BOKHARI-FRIBERG ET AL. 7 of 18

25724525, 2025, 7, Downloaded from https://agupubs.onlinelibrary.wiley.com/doi/10.1029/2024PA004995 by British Geological Survey, Wiley Online Library on [03102025]. See the Terms and Conditions (https://onlinelibrary.wiley.com/emms

and-conditions) on Wiley Online Library for rules of use; OA articles are governed by the applicable Creative

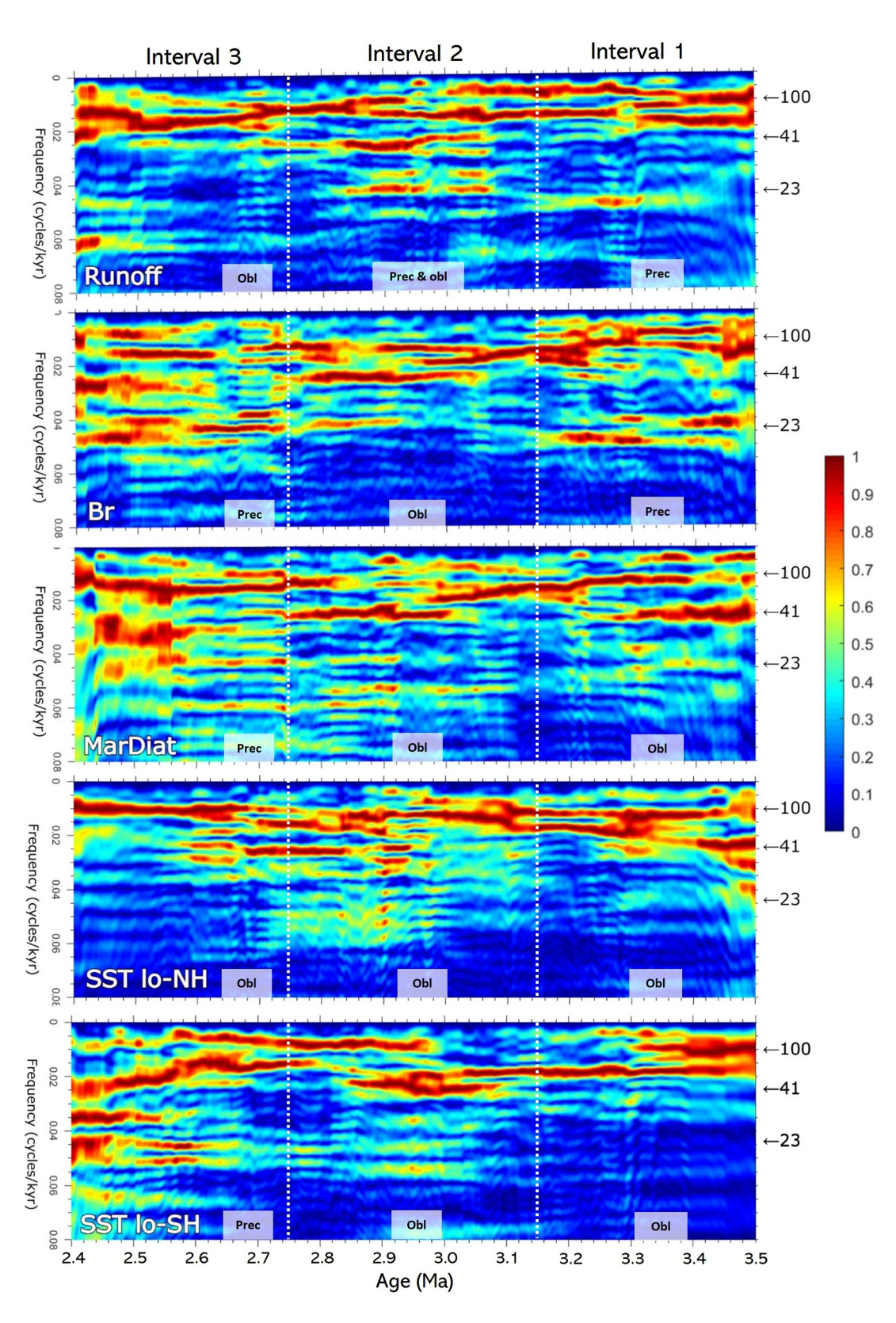


Figure 3.

BOKHARI-FRIBERG ET AL. 8 of 18



10.1029/2024PA004995

marine source via in situ productivity, corroborating its status as a reliable (siliceous) productivity indicator at Site U1445.

However, the relationship between Br and marine diatom abundance exhibits some inconsistency within the 2.5–2.3 Ma period, coinciding with a decrease in diatom abundance (Figure 2e). This decoupling could potentially be attributed to shifts in the dominant source of marine organic matter to which Br is bound or could be related to differential preservation of diatom valves. It is conceivable that a transition occurred from a siliceous (e.g., diatom) to a more calcareous (e.g., foraminifera and coccolithophore) productivity regime, possibly beginning ~2.65 Ma. This inference is supported by the observed increase in the ratio between coarse and fine sediment fraction during this period (Figure S10C in Supporting Information S1). Alternatively, changes in diatom preservation after 2.5 Ma may have influenced the observed relationship between Br and marine diatom abundance. Despite these nuances in the 2.5–2.3 Ma section of the record, the overall consistency of bulk sediment Br as a productivity proxy at Site U1445 is reaffirmed during the 3.5–2.5 Ma interval, and we proceed to interpret it as such throughout the remainder of this discussion.

4.2. Glacial-Interglacial ISM Runoff Variations and Their Influence on Marine Productivity

Our analysis highlights an inverse relationship between ISM runoff and marine productivity at Site U1445 at glacial-interglacial timescales across most of the study interval (Figures 2c and 2e, Figure S9 in Supporting Information S1). This intricate connection suggests a causal link between these two environmental parameters, where periods of elevated ISM runoff into the BoB are associated with diminished marine productivity. The inverse relationship between runoff and marine productivity in coastal regions has mainly been discussed within the context of two competing arguments: (a) heavy runoff increases marine productivity due to the increased nutrient supply (J. Li et al., 2023; Tapia et al., 2021), or (b) heavy runoff reduces marine productivity due to turbidity and/or a thicker freshwater surface layer inhibiting upwelling of nutrient-rich water to the surface (Jacob et al., 2018; Liess et al., 2015; Rayner et al., 2003). In the modern BoB, productivity is inhibited during episodes of strong monsoon seasonal runoff, following the continental rainfall during the summer months (June, July, August). The monsoon river runoff brings large volumes of freshwater ($\sim 1.6 \times 10^{12} \,\mathrm{m}^3\,\mathrm{yr}^{-1}$; Subramanian, 1993) and sediment to the bay area, which causes strong upper water column stratification and low light availability, hindering primary productivity (Ittekkot et al., 2003; Prasanna Kumar et al., 2002, 2010). A similar inverse relationship between U1445 runoff and productivity has been found in this study on glacial-interglacial timescales (Figures 2b, 2c, 2e and Figures S8 and S9 in Supporting Information S1), Warm interglacials had strong summer monsoon runoff input and decreased marine diatom abundance (productivity) and, conversely, cold glacials had reduced runoff and increased marine diatom abundance. This observed glacial (interglacial) trend suggests that the reduced (increased) freshwater and sediment input caused weak (strong) stratification and greater (lesser) light availability due to less (more) sediment supply to support (limit) marine biological productivity. Furthermore, we find that these glacial periods witnessed corresponding larger interhemispheric temperature gradients to provide strengthening of the zonal wind system (Crowley & North, 1991). These windier glacial periods witnessing reduced runoff conditions could have helped erode weak stratification to provide subsurface nutrients to sustain marine diatom productivity. Modern coastal upwelling regions have been found to support diatom productivity, for example, along the Portuguese margin (Abrantes, 1988; Gil et al., 2007), California (Closset et al., 2021), and in the Benguela region (Etourneau et al., 2009). Therefore, we find that the Late Pliocene glacials presented ideal conditions for sustaining marine biological productivity when the runoff was reduced in the coastal BoB. This is opposite to modern conditions where increased runoff leads to stronger stratification, limiting nutrient availability to surface waters and consequently supressing marine productivity, especially during the summer months (Prasanna Kumar et al., 2002).

Figure 3. Evolutionary spectra of U1445 runoff, Br, and marine diatom (MarDiat) concentrations, as well as sea surface temperature (SST) low-to high-latitude Northern and Southern Hemisphere gradients between 2.4 and 3.5 Ma using Fast Fourier Transform. Important orbital frequencies are indicated with arrows: 100 kyr (eccentricity), 41 kyr (obliquity), 23 kyr (precession). The spectral analysis was applied continuously over the full 3.5–2.4 Ma interval. White lines have been added at key transitions based on visual interpretation (i.e., these do not represent separate spectral analyses), and the dominant frequency/frequencies in each interval is indicated in white text boxes. Data has been detrended to remove cyclicities larger than 200 kyr. SST data are from Sites 982 (Herbert et al., 2016), 662 (Herbert et al., 2010), and 1,090 (Martínez-García et al., 2010); see Figure S6 in Supporting Information S1.

BOKHARI-FRIBERG ET AL. 9 of 18

25724525, 2025, 7, Downloaded from https://agupubs.onlinelibrary.wiley.com/doi/10.1029/2024PA004995 by British Geological Survey, Wiley Online Library on [03/10/2025]. See the Terms and Conditions (https://onlinelibrary.wiley.

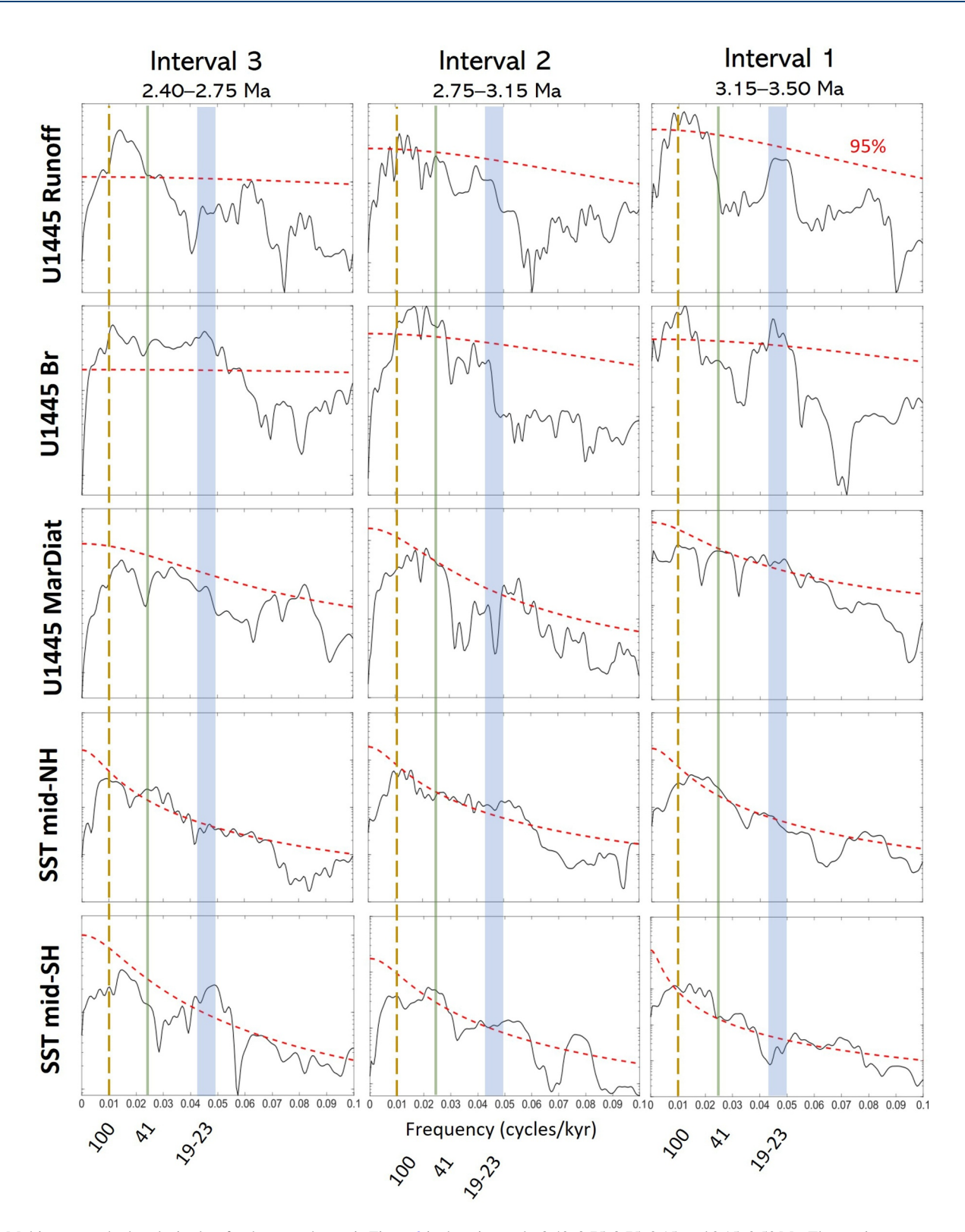


Figure 4. Multi-taper method analysis plots for the same data as in Figure 3 in three intervals: 2.40–2.75, 2.75–3.15, and 3.15–3.50 Ma. The *x*-axis represents power, and the *y*-axis frequency (cycles/unit). The red line represents 95% confidence. Solid vertical lines are placed at statistically significant orbital frequencies (obliquity 41 kyr, precession 19–23 kyr), while the 100-kyr eccentricity frequency is shown as a dotted line to indicate its expected location but acknowledge its lack of statistical significance due to the limited number of cycles within each analyzed window. See also Figure S7 in Supporting Information S1.

BOKHARI-FRIBERG ET AL. 10 of 18

4.3. Orbital Frequency and Phasing of ISM Runoff and Productivity

Spectral analyses conducted on climate proxy records offer valuable insights into the influence of orbital forcing on climate dynamics, for example, 100-kyr cycles have been established to control climate (including glacial cycles and Asian monsoon strength) in the Late Pleistocene ("100-kyr world") (Ao et al., 2023; Hobart et al., 2023; Liu et al., 2008; Tripathi et al., 2023; Zhou et al., 2023). Although fewer studies have been conducted in the Pliocene, growing evidence points to 100 kyr (eccentricity) pacing on climate processes, for example, a Southern Hemisphere influence on the East Asian Monsoon (Zhang et al., 2022) and the regional oceanography of the Southwest Pacific (Caballero-Gill et al., 2019). We also find evidence of persistent 100 kyr power in our ISM runoff and marine biological productivity records throughout most of the study interval (3.5–2.4 Ma) (Figure 3). The strong 100 kyr cyclicity is also present in the low-to-high latitude sea surface temperature (SST) gradients (Figure 3 and Figure S6 in Supporting Information S1). This observation is perhaps a reflection of highly variable icesheet growth and decline that were primarily controlled by obliquity but also being affected by eccentricity.

Precession via insolation has previously been found to dominate low-latitude climate in the Pliocene, including ISM rainfall (Thomson et al., 2021) and the West African monsoon (Bosmans et al., 2014; Cleaveland & Herbert, 2007; DeMenocal, 2004; Kuechler et al., 2018; Prell & Kutzbach, 1992; Ruddiman et al., 1986; Tiedemann et al., 1994). In interval 1, we find precession dominance on the runoff record as expected. From interval 2 (~3.15 Ma), however, obliquity pacing begins to appear in ISM runoff after the onset of NH icesheet growth aligned with the observed low-to-high NH SST gradient (Figures 3 and 4). After 2.8 Ma, transition to stronger obliquity control on runoff is similar to the one observed in other low latitude climate following the establishment of NHG (Bailey et al., 2013; Blake-Mizen et al., 2019; Jansen et al., 2000; Raymo, 1994; Shackleton et al., 1984), suggesting an increasing NH influence on low-latitude climate with growing NH ice sheets. Following the establishment of NHG, amplified obliquity forcing caused an enhanced interhemispheric temperature contrast in the NH. Increased NH ice sheet formation could have influenced atmospheric circulation patterns, including the strength and direction of trade winds, thereby affecting the position of the intertropical convergence zone (ITCZ), which plays a crucial role in the distribution of rainfall, runoff, and wind associated with the modern ISM and the West African Monsoon. Obliquity control during the colder Pleistocene has also been observed for ISM rainfall/ runoff (Gebregiorgis et al., 2018) and the West African Monsoon (Tiedemann et al., 1994). While the effect of NH ice sheet on Pleistocene ISM rainfall/runoff has been hypothesized (Clemens et al., 2021), our records show that the NH influence on the low-latitude monsoon hydroclimate may have intensified post ~3.15 Ma following the onset of NHG. Furthermore, the varying degrees of obliquity (Intervals 1 and 2) and precession (Interval 3) power on productivity records indicate high-latitude influence until ~2.75 Ma.

Runoff and productivity show somewhat similar relative powers in the obliquity and precession spectra in Intervals 1 (3.50–3.15 Ma) and 2 (3.15–2.75 Ma) (Figure 4) suggesting a possible orbital coupling between runoff and productivity in the Late Pliocene. The relationship differs dramatically in Interval 3 (2.75–2.40) however, which is also where they show a less consistent coupling (see Figure S9 in Supporting Information S1, top panel). The multiple strong frequencies present in Interval 3 of both Br and marine diatom are reminiscent of those in low-to-high latitude SH SST gradient (Figure 3), rather than those in low-to-high NH, suggesting a stronger SH impact on marine biological productivity in the initial part of the Early Pleistocene. Contrary to the aforementioned low-latitude (e.g., West African monsoon) climate records, no evident switch from precession to obliquity is observed in the ISM runoff (thermodynamic component) or productivity (dynamic component) records. Though runoff does display strengthened obliquity frequency in Intervals 2 and 3, it manifests as short-lived transitions rather than a switch. Thus, these observations affirm that the ISM is a more complex monsoon system (Thomson et al., 2021) than that of the West African monsoon, which is primarily influenced by Atlantic Ocean dynamics, serving as a direct pathway for moisture transport (Raj et al., 2019). The presence of landmasses between the BoB and the NH ice sheets may hinder the direct transmission of monsoonal effects to high-latitude climates, complicating the relationship between ISM dynamics and NH climatic patterns (Jalihal et al., 2020). This is possibly the reason why an indirect teleconnection between ISM dynamics and NH climate has commonly been suggested for the Holocene (Naidu et al., 2020) than a more direct effect ascertained using palaeoclimate

To further understand the interplay between the proxies and their timings in the obliquity and precession bands, the phasing of U1445 runoff, Br, and marine diatoms are illustrated in a phase wheel (Figure 5; see figure caption for details). The phase analysis of the productivity proxies (Br and marine diatom) demonstrates a consistent in-

BOKHARI-FRIBERG ET AL. 11 of 18

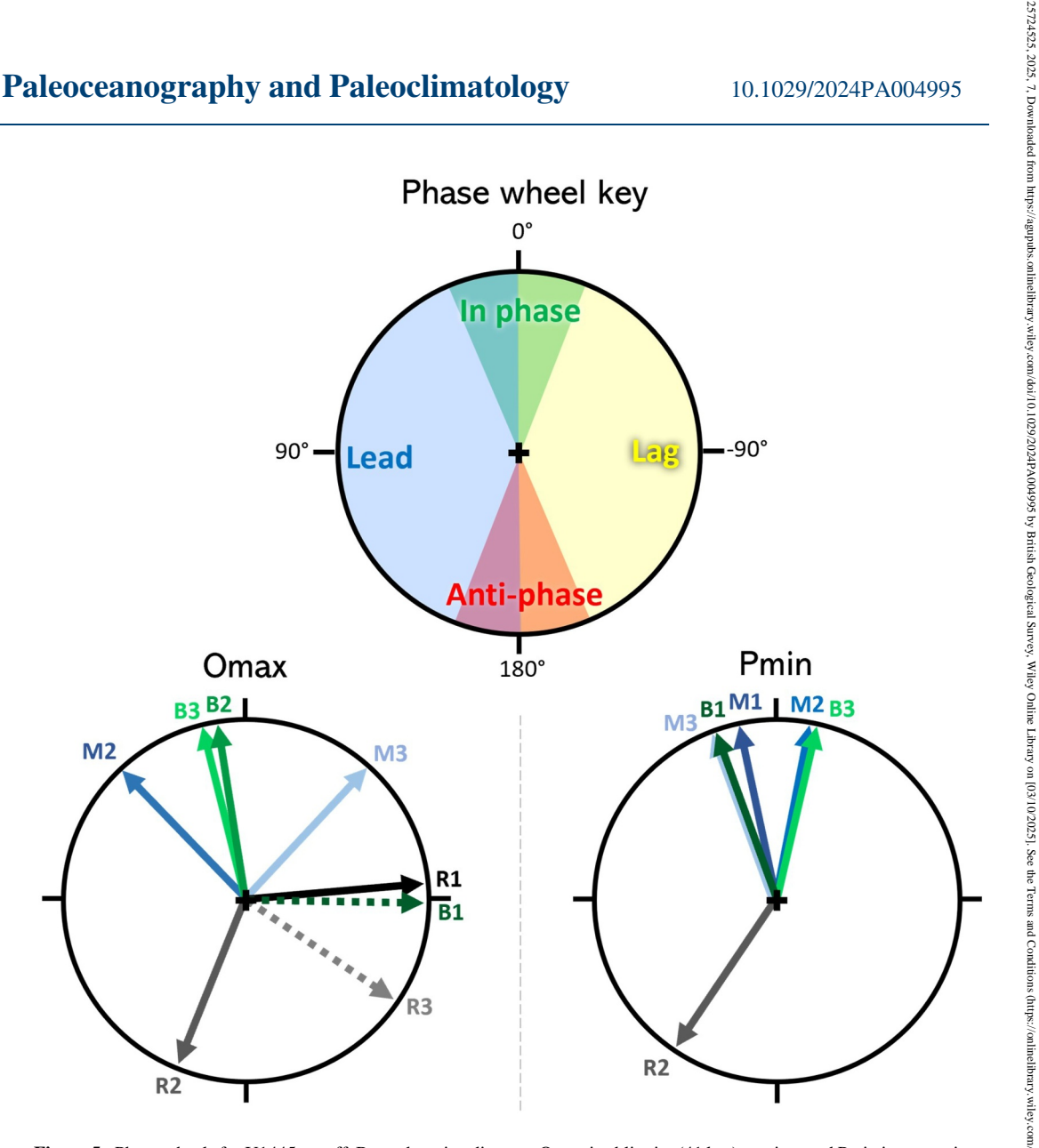


Figure 5. Phase wheels for U1445 runoff, Br, and marine diatoms. Omax is obliquity (41 kyr) maxima and Pmin is precession (23 kyr) minima. The precession index is defined as $\Delta e \sin \varpi$ where ϖ is the longitude of perihelion measured from the moving vernal point and e is the eccentricity of Earth's orbit about the Sun. R1, R2, and R3 (black/gray) represent runoff maxima; B1, B2, and B3 (green) represent Br maxima; and M1, M2, and M3 (blue) represent marine diatom maxima in Intervals 1 (3.15–3.50 Ma), 2 (2.75–3.15 Ma), and 3 (2.40–2.75 Ma), respectively. Coherence <0.38 is not plotted, 0.38–0.50 is plotted with dotted arrows, and >0.50 is plotted with filled arrows. Arrows pointing up (down) indicate an in-phase (antiphase) relationship with Omax/Pmin, whereas those pointing to the right (left) indicate a lag (lead). See Table S4 in Supporting Information S1 for coherence and phase values.

phase relationship with precession minima (P_{\min}) and obliquity maxima (O_{\max}), particularly evident in the precession band. This phasing highlights a strong sensitivity of marine productivity to NH insolation forcing, indicating that these proxies are strongly controlled by the timing of orbital variations. The runoff proxy, however, displays a more complex phasing, with vaguely anti-phased behavior in the obliquity band and low correlation in the precession band during most intervals. This differing Pliocene response between ISM rainfall/ runoff and wind driven productivity at the P_{\min} and O_{\max} bands contrasts with findings from the late Quaternary (Clemens et al., 2021; Gebregiorgis et al., 2018), where ISM rainfall/runoff, though showing some precessionband coherence (linked to cross-equatorial winds), was more strongly modulated by obliquity and internal forcings such as Southern Hemisphere warming and ice volume change.

This complexity is further illustrated by examining the relationship between runoff and productivity phasing across the obliquity and precession bands. In the obliquity band, R2 and B2 exhibit an anti-phased relationship, while in the precession band, the correlation between runoff and precession is generally low, particularly outside

BOKHARI-FRIBERG ET AL. 12 of 18 Interval 2. These results suggest that NH summer insolation minima (colder summers) coincided with reduced ISM rainfall and runoff, which in turn enhanced BoB productivity. This anti-phased relationship between runoff and productivity is consistent with the previously discussed inferences that reduced stratification promoted higher productivity during low-runoff periods. Notably, the strongest inverse coupling between runoff and productivity occurs in Interval 2 (2.75–3.15 Ma), when productivity is at its highest and runoff is most subdued (Figures 2c and 2e). The contrasting phase relationships between runoff and productivity proxies provide a framework for hypothesizing ISM sensitivity to external versus internal forcings. The in-phase behavior of productivity proxies with precession-driven insolation supports a dominant role of NH orbital forcing in driving marine productivity. Conversely, the anti-phased or weakly correlated runoff signals suggest a potential decoupling from NH insolation, implicating internal dynamics, such as shifts in the ITCZ, or external Southern Hemisphere influences. These findings underscore the complexity of ISM dynamics during the Pliocene, potentially reflecting a greater influence of internal climate feedbacks or a distinct sensitivity to regional forcings during this period.

4.4. ISM Runoff and Productivity During the Mid-Piacenzian Warm Period

The mid-Piacenzian Warm Period (mPWP; 3.025–3.264 Ma) marks an interval of higher CO₂ concentrations and a warmer climate (temperatures 2–3°C higher than preindustrial times) and is thus a useful analog for future climate scenario (Dowsett et al., 2016). Factors such as elevated temperatures, altered oceanic circulation patterns, and modified land-sea temperature gradients likely contributed to shifts in monsoonal intensity and rainfall patterns across the Indian subcontinent (Katzenberger et al., 2021). Past studies of mPWP ISM have simulated stronger rainfall during interglacials with stronger precession forcing attributed to increased summer surface air temperatures (Prescott et al., 2019). However, the opposite is observed in our records. We reveal a notable increase in ISM runoff/rainfall (Figure 6c) during the warming phase (B) from M2 (3.30 Ma) to shortly after M1 (3.24 Ma) in a period of low precession and eccentricity variability (A). This trend is succeeded by a decrease in runoff concurrent with an increase in precession and eccentricity amplitude until post-KM2 (3.11 Ma). Notably, the KM3 interglacial, aligning with strong precession, stands out as the period with the weakest runoff in the entire mPWP (Figures 6a–6c), during sustained low productivity (D—please note the inversion).

While productivity generally exhibits an inverse correlation with runoff, reaffirming the typical rainfall-productivity dynamics at Site U1445, nuances emerge after \sim 3.09 Ma. Here, the previously distinct relationship between G-IG cycles and ISM rainfall, as well as between rainfall and productivity, begin to weaken. In this interval, a notable peak in productivity (3.07–3.08 Ma) coincides with stable/muted runoff levels. Interestingly, this low runoff/rainfall amplitude aligns with a phase of heightened variability in eccentricity and precession relative to much of the older part of the interval (A). This divergence from global climatic drivers might be attributed to a predominant influence of local factors over broader regional or global factors. This is exemplified by the atypical benthic δ^{18} O pattern at Site U1445 between 3.09 and 3.025 Ma, which diverges from the global benthic stack LR04. This incongruity suggests that Site U1445's rainfall regime follows a unique rhythm during this interval, both in the benthic realm and, presumably, in surface conditions.

In contrast to our findings, previous studies point to a clear link between precession forcing and ISM strength in the Pliocene (Clemens & Prell, 1990; Thomson et al., 2021). The ambiguity and lack of consistency in ISM proxies underscore the necessity of continued Pliocene ISM studies for reliable results in this crucial region and period. Furthermore, as mPWP simulations employ a modern orbital arrangement (Prescott et al., 2019), investigating the impact of orbital forcings on ISM through paleoclimate proxies and using Pliocene-specific orbital calculations is imperative for a comprehensive understanding of past ISM dynamics. More work is needed to draw accurate comparisons between proxies and model-based past climate reconstructions to better assess and apply process-based knowledge about the Earth System at the end of this century. The quoted literature, and our findings here, emphasize the complex interplay of climate boundary conditions on monsoon responses to solar insolation, cautioning against oversimplified assumptions that monsoon strengthens during interglacials or weakens during glacial times.

5. Conclusions

This study investigates the intricate relationship between ISM rainfall/runoff and productivity changes through multi-proxy climate reconstructions on orbital timescales across the Late Pliocene and Early Pleistocene (3.5–2.4 Ma). By analyzing high-resolution runoff (XRF elemental data at 100–200 years resolution) and productivity

BOKHARI-FRIBERG ET AL. 13 of 18

25724525, 2025, 7, Downloaded from https://agupubs.onlinelibrury.wiley.com/doi/10.1029/2024PA004995 by British Geological Survey, Wiley Online Library on [03/10/2025]. See the Terms and Conditions (https://agupubs.onlinelibrury.wiley.com/doi/10.1029/2024PA004995 by British Geological Survey, Wiley Online Library on [03/10/2025]. See the Terms and Conditions (https://agupubs.onlinelibrury.wiley.com/doi/10.1029/2024PA004995 by British Geological Survey, Wiley Online Library on [03/10/2025]. See the Terms and Conditions (https://agupubs.onlinelibrury.wiley.com/doi/10.1029/2024PA004995 by British Geological Survey, Wiley Online Library on [03/10/2025]. See the Terms and Conditions (https://agupubs.onlinelibrury.wiley.com/doi/10.1029/2024PA004995 by British Geological Survey, Wiley Online Library on [03/10/2025]. See the Terms and Conditions (https://agupubs.onlinelibrury.wiley.com/doi/10.1029/2024PA004995 by British Geological Survey, Wiley Online Library on [03/10/2025]. See the Terms and Conditions (https://agupubs.onlinelibrury.wiley.com/doi/10.1029/2024PA004995 by British Geological Survey, Wiley Online Library on [03/10/2025]. See the Terms and Conditions (https://agupubs.onlinelibrury.wiley.com/doi/10.1029/2024PA004995 by British Geological Survey, Wiley Online Library on [03/10/2025]. See the Terms and Conditions (https://agupubs.onlinelibrury.wiley.com/doi/10.1029/2024PA004995 by British Geological Survey, Wiley Online Library on [03/10/2024].

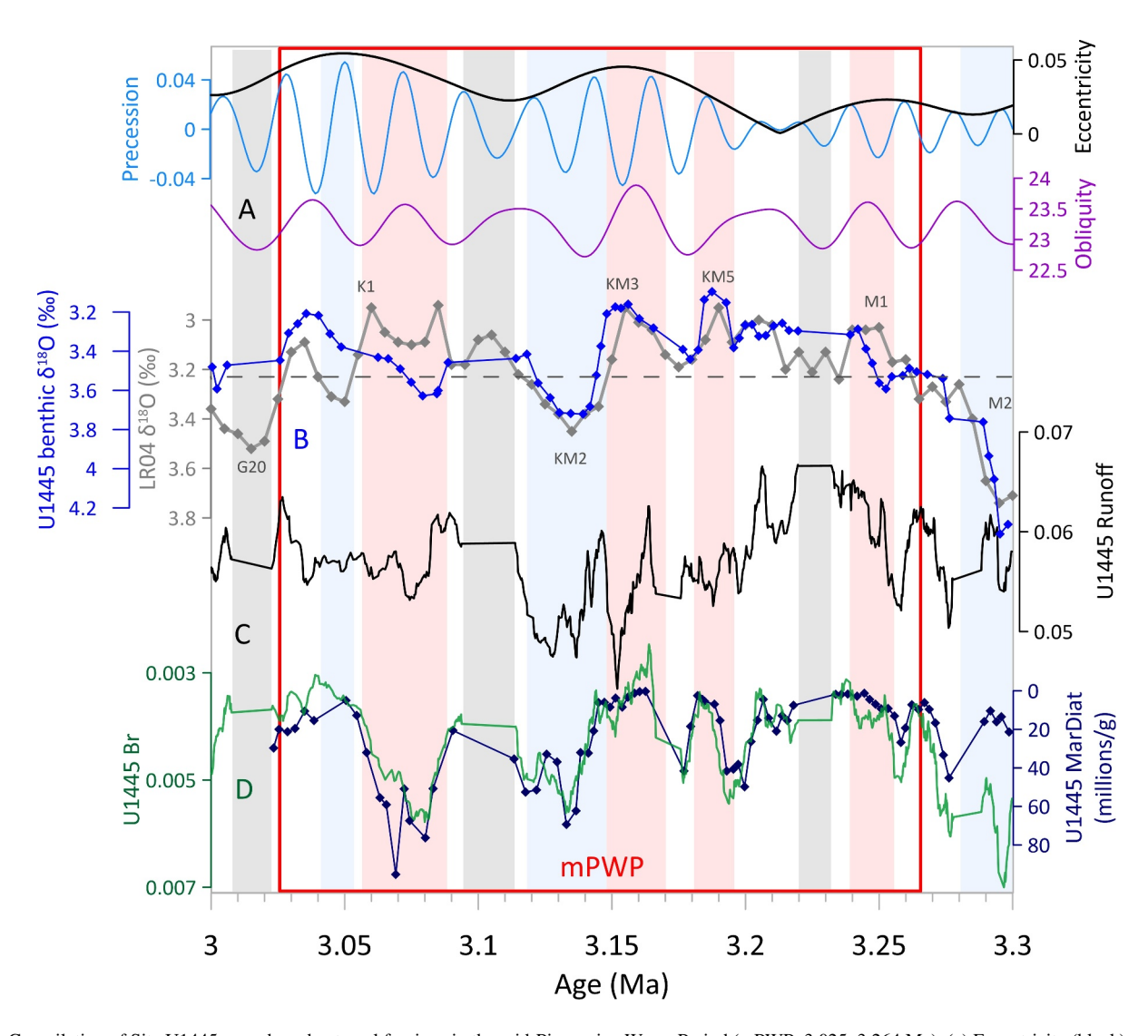


Figure 6. Compilation of Site U1445 records and external forcings in the mid-Piacenzian Warm Period (mPWP; 3.025-3.264 Ma). (a) Eccentricity (black), precession (blue) and obliquity (purple) (Laskar, 2004). (b) LR04 (gray) and U1445 (blue) benthic $\delta180$ (‰) with modern value (3.23%) as a gray dotted line. (c) U1445 runoff (black). (d) U1445 Br (green) and marine diatom concentration (millions/g) (blue); inverted for easier comparison. Warm and cold periods are highlighted in red and blue, respectively. Gray highlighted areas denote gaps in the data.

(XRF-Br and marine diatom concentration) proxy records from the northwestern BoB, we demonstrate that a relationship between ISM runoff and marine biological productivity existed in the northern BoB during the study period. Reduced runoff conditions during glacials allowed for well-mixed upper water columns and limited turbidity, enabling enhanced biological productivity. In contrast, increased rainfall and runoff during interglacials caused upper water column stratification and turbidity, hindering biological productivity, as observed in the modern.

We demonstrate the reliability of XRF-derived Br counts as a productivity proxy at Site U1445, showing a strong correlation with marine (diatom) productivity throughout the Late Pliocene to the earliest Pleistocene. While some inconsistencies are observed within specific intervals, the overall coherence reaffirms Br as a robust indicator of (siliceous) biological productivity in this setting.

Spectral analyses reveal the influence of orbital forcing on ISM dynamics, with eccentricity, obliquity, and precession playing significant roles in modulating ISM runoff and productivity variability during the study interval. These orbital parameters exert control over ISM rainfall patterns and productivity through complex interactions with regional and global climate systems and vary in their proportional influence on the ISM through the Late Pliocene. We found strong obliquity control on ISM rainfall/runoff after the onset of NH ice sheets (after

BOKHARI-FRIBERG ET AL. 14 of 18

15 of 18



Acknowledgments

P. Anand would like to thank the Open

Environment Research Council Isotope

University for the studentship and Natural

Geoscience Facility grant (IP-1839-1118)

for funding support to Y. Bokhari Friberg.

K. Littler acknowledges support from an

N012100/1) and the Camborne School of

Mines Trust. Funding for M.M. Robinson

Survey Ecosystems Land Change Science

Program. Any use of trade, firm, or product

names is for descriptive purposes only and

does not imply endorsement by the U.S.

German Science Foundation for financial

Government. OE Romero thanks the

support.

was provided by the U.S. Geological

UKIODP Moratorium Grant (NE/

Paleoceanography and Paleoclimatology

10.1029/2024PA004995

3.15 Ma). However, this relationship is less straight-forward than observed in many other low-latitude climate records, such as the West African monsoon. Our phase analysis confirmed strongest runoff-productivity inverse coupling in Interval 2 (2.75-3.15 Ma), when productivity is at its highest and runoff is most subdued within the study interval.

Our study highlights the value of integrating spectral, wavelet, and phase analyses as complementary approaches to disentangle the interplay of ISM dynamics and orbital forcing. The consistent phasing of productivity proxies with precession and obliquity supports the hypothesis of NH insolation control, particularly for marine productivity. However, variability in runoff phasing underscores the influence of additional factors, including internal feedbacks and potential Southern Hemisphere-driven teleconnections. These results, showing a decoupling between ISM rainfall/runoff and wind-driven productivity at the P_{\min} (and O_{\max}) band(s), contrast with late Pleistocene findings where ISM rainfall/runoff exhibited some precession-band coherence, but were more strongly modulated by obliquity and internal forcings. These findings thereby refine our understanding of ISM (rainfall/runoff and wind) variability during the Plio-Pleistocene, emphasizing the need to consider the influence of multiple mechanisms in future reconstructions and climate model comparisons.

Furthermore, our investigation into the mPWP provides insights into the response of the ISM rainfall/runoff to elevated CO₂ concentrations and warmer temperatures, serving as a useful analog for future climate. While past studies have suggested a strengthening of ISM rainfall during interglacial periods with increased precession forcing, our findings reveal nuanced responses, with variability in ISM runoff and productivity suggesting a complex interplay of local and global climate factors, including the modulation of glacialinterglacial cycles.

This study underscores the importance of continued research into Pliocene ISM dynamics to improve our understanding of past climate variability and to gain process-based knowledge to inform future climate projections. By unraveling the complexities of ISM runoff and productivity dynamics and their relationships with different forcings, we can better assess the vulnerability of monsoon-dependent regions to ongoing climate change and refine predictions of future monsoon behavior.

Data Availability Statement

The data set supporting the findings of this study are archived in Figshare and are freely available under the Creative Commons Attribution 4.0 International License (CC BY 4.0). The data set is cited in the references as Bokhari-Friberg et al. (2025).

References

Abrantes, F. (1988). Diatom assemblages as upwelling indicators in surface sediments off Portugal. Marine Geology, 85(1), 15-39. https://doi.org/ 10.1016/0025-3227(88)90082-5

Ahn, S., Khider, D., Lisiecki, L. E., & Lawrence, C. E. (2017). A probabilistic Pliocene–Pleistocene stack of benthic δ18O using a profile hidden Markov model. Dynamics and Statistics of the Climate System, 2(1), 1-16. https://doi.org/10.1093/climsys/dzx002

Annamalai, H. (2007). IPCC climate models and the Asian summer monsoon. IPRC Climate, 7(2), 10-14.

Ao, H., Rohling, E. J., Li, X., Song, Y., Roberts, A. P., Han, Y., et al. (2023). Northern hemisphere ice sheet expansion intensified Asian aridification and the winter monsoon across the mid-Pleistocene transition. Communications Earth & Environment, 4(1), 1-11. https://doi.org/10. 1038/s43247-023-00686-9

Bailey, I., Hole, G. M., Foster, G. L., Wilson, P. A., Storey, C. D., Trueman, C. N., & Raymo, M. E. (2013). An alternative suggestion for the Pliocene onset of major northern hemisphere glaciation based on the geochemical provenance of North Atlantic Ocean ice-rafted debris. Ouaternary Science Reviews, 75, 181-194. https://doi.org/10.1016/j.quascirev.2013.06.004

Banerji, U. S., Joshi, K. B., Pandey, L., & Dubey, C. P. (2022). An outline of geochemical proxies used on marine sediments deposited during the Quaternary Period. In Stratigraphy and Timescales (1st ed., Vol. 7, pp. 1-35). Elsevier Inc. https://doi.org/10.1016/bs.sats.2022.09.002

Berends, C. J., De Boer, B., & Van De Wal, R. S. W. (2021). Reconstructing the evolution of ice sheets, sea level, and atmospheric CO2 during the past 3.6 million years (pp. 361-377).

Blake-Mizen, K., Hatfield, R. G., Stoner, J. S., Carlson, A. E., Xuan, C., Walczak, M., et al. (2019). Southern Greenland glaciation and western boundary undercurrent evolution recorded on Eirik Drift during the late Pliocene intensification of northern hemisphere glaciation. Quaternary Science Reviews, 209, 40-51. https://doi.org/10.1016/j.quascirev.2019.01.015

Bloemendal, J., & DeMenocal, P. (1989). Evidence for a change in the periodicity of tropical climate cycles at 2.4 Myr from whole-core magnetic susceptibility measurements. Nature, 342(6252), 897-900. https://doi.org/10.1038/342897a0

Bokhari-Friberg, Y., Anand, P., Romero, O., Littler, K., Robinson, M., Sexton, P., et al. (2025). Bokhari-Friberg et al. - "Influence of Indian Summer Monsoon on Marine Biological Productivity Across the Late Pliocene and Early Pleistocene" [Dataset]. Figshare. https://doi.org/10. 6084/m9.figshare.29287514

Bosmans, J. H. C., Drijfhout, S. S., Tuenter, E., Hilgen, F. J., & Lourens, L. J. (2014). Response of the North African summer monsoon to precession and obliquity forcings in the EC-Earth GCM. Climate Dynamics, 44(1-2), 279-297. https://doi.org/10.1007/s00382-014-2260-z

BOKHARI-FRIBERG ET AL.



- 10.1029/2024PA004995
- Bradtmiller, L. I., Anderson, R. F., Fleisher, M. Q., & Burckle, L. H. (2006). Diatom productivity in the equatorial Pacific ocean from the last glacial period to the present: A test of the silicic acid leakage hypothesis. *Paleoceanography*, 21(4), 1–12. https://doi.org/10.1029/2006PA001282
- Caballero-Gill, R. P., Herbert, T. D., & Dowsett, H. J. (2019). 100-kyr paced climate change in the Pliocene warm period, Southwest Pacific. Paleoceanography and Paleoclimatology, 34(4), 524–545. https://doi.org/10.1029/2018PA003496
- Cai, M., Xu, Z., Clift, P. D., Khim, B.-K., Lim, D., Yu, Z., et al. (2018). Long-term history of sediment inputs to the eastern Arabian Sea and its implications for the evolution of the Indian summer monsoon since 3.7 Ma. *Geological Magazine*, 2013(6), 1–12. https://doi.org/10.1017/s0016756818000857
- Chen, Z., Zhou, T., Zhang, L., Chen, X., Zhang, W., & Jiang, J. (2020). Global land monsoon precipitation changes in CMIP6 projections. Geophysical Research Letters, 47(14), e2019GL086902. https://doi.org/10.1029/2019GL086902
- Cleaveland, L. C., & Herbert, T. D. (2007). Coherent obliquity band and heterogeneous precession band responses in early Pleistocene tropical sea surface temperatures. *Paleoceanography*, 22(2), 1–13. https://doi.org/10.1029/2006PA001370
- Clemens, S. C., Yamamoto, M., Thirumalai, K., Giosan, L., Richey, J. N., Nilsson-Kerr, K., et al. (2021). Remote and local drivers of pleistocene South Asian summer monsoon precipitation: A test for future predictions. *Science Advances*, 7(23), 1–16. https://doi.org/10.1126/sciadv.abg3848
- Clemens, S. C., Kuhnt, W., LeVay, L. J., Anand, P., Ando, T., Bartol, M., et al. (2016). Site U1445. Proceedings of the International Ocean Discovery Program, 353(July). https://doi.org/10.14379/iodp.proc.353.105.2016
- Clemens, S. C., Murray, D. W., & Prell, W. L. (1996). Nonstationary phase of the Plio-pleistocene Asian monsoon. Science, 274(November), 943–948. https://doi.org/10.1126/science.274.5289.943
- Clemens, S. C., & Prell, W. L. (1990). Late Pleistocene variability of Arabian Sea summer monsoon winds and continental aridity: Eolian records from the lithogenic component of deep-sea sediments. *Paleoceanography*. 5(2), 109–145, https://doi.org/10.1029/pa005i002p00109
- Clemens, S. C., Prell, W. L., Sun, Y., Liu, Z., & Chen, G. (2008). Southern hemisphere forcing of Pliocene δ18O and the evolution of Indo-Asian monsoons. *Paleoceanography*, 23(4), 1–15. https://doi.org/10.1029/2008PA001638
- Clift, P. D., Hodges, K. V., Heslop, D., Hannigan, R., Van Long, H., & Calves, G. (2008). Correlation of Himalayan exhumation rates and Asian monsoon intensity. *Nature Geoscience*, 1(12), 875–880. https://doi.org/10.1038/ngeo351
- Closset, I., McNair, H. M., Brzezinski, M. A., Krause, J. W., Thamatrakoln, K., & Jones, J. L. (2021). Diatom response to alterations in upwelling and nutrient dynamics associated with climate forcing in the California Current System. *Limnology & Oceanography*, 66(4), 1578–1593. https://doi.org/10.1002/lno.11705
- Crowley, T. J., & North, G. R. (1991). Paleoclimatology. Oxford University Press.
- Curray, J. R., Emmel, F. J., & Moore, D. G. (2002). The Bengal Fan: Morphology, geometry, stratigraphy, history and processes. *Marine and Petroleum Geology*, 19(10), 1191–1223. https://doi.org/10.1016/S0264-8172(03)00035-7
- De la Vega, E., Chalk, T. B., Wilson, P. A., Bysani, R. P., & Foster, G. L. (2020). Atmospheric CO2 during the mid-Piacenzian Warm Period and the M2 glaciation. *Scientific Reports*, 10(1), 1–9. https://doi.org/10.1038/s41598-020-67154-8
- DeMenocal, P. B. (2004). African climate change and faunal evolution during the Pliocene-Pleistocene. *Earth and Planetary Science Letters*, 220(1–2), 3–24. https://doi.org/10.1016/S0012-821X(04)00003-2
- Dowsett, H., Dolan, A., Rowley, D., Moucha, R., Forte, A. M., Mitrovica, J. X., et al. (2016). The PRISM4 (mid-Piacenzian) paleoenvironmental reconstruction. Climate of the Past, 12(7), 1519–1538. https://doi.org/10.5194/cp-12-1519-2016
- Etourneau, J., Martinez, P., Blanz, T., & Schneider, R. (2009). Pliocene-Pleistocene variability of upwelling activity, productivity, and nutrient cycling in the Benguela region. *Geology*, 37(10), 871–874. https://doi.org/10.1130/G25733A.1
- Gebregiorgis, D., Giosan, L., Hathorne, E. C., Anand, P., Nilsson-Kerr, K., Plass, A., et al. (2020). What can we learn from X-ray fluorescence core scanning data? A paleomonsoon case study. *Geochemistry*, *Geophysics*, *Geosystems*, 21(2), 1–17. https://doi.org/10.1029/2019GC008414
- Gebregiorgis, D., Hathorne, E. C., Giosan, L., Clemens, S., Nürnberg, D., & Frank, M. (2018). Southern Hemisphere forcing of South Asian monsoon precipitation over the past ~1 million years. *Nature Communications*. 9(1), 4702. https://doi.org/10.1038/s41467-018-07076-2
- Geirsdottir, A., & Eiriksson, J. (1994). Growth of intermittent ice sheet in Iceland during the late Pliocene and early pleistocene. *Quaternary Research*, 42(2), 115–130. https://doi.org/10.1006/qres.1994.1061
- Gil, I. M., Abrantes, F., & Hebbeln, D. (2007). Diatoms as upwelling and river discharge indicators along the Portuguese margin: Instrumental data linked to proxy information. The Holocene, 17(8), 1245–1252. https://doi.org/10.1177/0959683607085131
- Gilfedder, B. S., Petri, M., Wessels, M., & Biester, H. (2011). Bromine species fluxes from Lake Constance's catchment, and a preliminary lake mass balance. Geochimica et Cosmochimica Acta, 75(12), 3385–3401. https://doi.org/10.1016/j.gca.2011.03.021
- Gupta, A. K., & Thomas, E. (2003). Initiation of Northern Hemisphere glaciation and strengthening of the northeast Indian monsoon: Ocean drilling program site 758, eastern equatorial Indian Ocean. Geology, 31(1), 47–50. https://doi.org/10.1130/0091-7613(2003)031<0047: IONHGA>2.0.CO:2
- Gupta, A. K., Yuvaraja, A., Prakasam, M., Clemens, S. C., & Velu, A. (2015). Evolution of the South Asian monsoon wind system since the late middle miocene. *Palaeogeography*, *Palaeoclimatology*, *Palaeoecology*, 438, 160–167. https://doi.org/10.1016/j.palaeo.2015.08.006
- Ha, K. J., Moon, S., Timmermann, A., & Kim, D. (2020). Future changes of summer monsoon characteristics and evaporative demand over Asia in CMIP6 simulations. *Geophysical Research Letters*, 47(8), 1–10. https://doi.org/10.1029/2020GL087492
- Haywood, A. M., Dowsett, H. J., & Dolan, A. M. (2016). Integrating geological archives and climate models for the mid-Pliocene warm period. *Nature Communications*, 7(May 2015), 1–14. https://doi.org/10.1038/ncomms10646
- Herbert, T. D., Lawrence, K. T., Tzanova, A., Peterson, L. C., Caballero-Gill, R., & Kelly, C. S. (2016). Late Miocene global cooling and the rise of modern ecosystems. *Nature Geoscience*, 9(11), 843–847. https://doi.org/10.1038/ngeo2813
- Herbert, T. D., Peterson, L. C., Lawrence, K. T., Herbert, T. D., Peterson, L. C., Lawrence, K. T., & Liu, Z. (2010). Tropical Ocean temperatures over the past 3.5 million years. Science, 328(5985), 1530–1534. https://doi.org/10.1126/science.1185435
- Hobart, B., Lisiecki, L. E., Rand, D., Lee, T., & Lawrence, C. E. (2023). Late Pleistocene 100-kyr glacial cycles paced by precession forcing of summer insolation. *Nature Geoscience*, 16(8), 717–722. https://doi.org/10.1038/s41561-023-01235-x
- Huang, Y., Clemens, S. C., Liu, W., Wang, Y., & Prell, W. L. (2007). Large scale hydrological change drove the late miocene C4 plant expansion in the Himalayan foreland Arabian Peninsula. Geology, 35(6), 531–534. https://doi.org/10.1130/G23666A.1
- Ittekkot, V., Kudrass, H.-R., Quadfasel, D., & Unger, D. (2003). The bay of Bengal. Deep-Sea Research. Part 2. Topical Studies in Oceanography, 50(5), 853–1054.
- Jacob, B. G., Tapia, F. J., Quiñones, R. A., Montes, R., Sobarzo, M., Schneider, W., et al. (2018). Progress in Oceanography Major changes in diatom abundance, productivity, and net community metabolism in a windier and dryer coastal climate in the southern Humboldt Current. Progress in Oceanography, 168(October), 196–209. https://doi.org/10.1016/j.pocean.2018.10.001

BOKHARI-FRIBERG ET AL. 16 of 18

- Jalihal, C., Srinivasan, J., & Chakraborty, A. (2020). Different precipitation response over land and ocean to orbital and greenhouse gas forcing. Scientific Reports, 10(1), 1–11. https://doi.org/10.1038/s41598-020-68346-y
- Jansen, E., Frontval, T., Rack, F., & Channell, J. E. T. (2000). Pliocene-Pleistocene ice rafting history and cyclicity in the Nordic Seas during the last 3.5 Myr. Paleoceanography, 15(6), 709–721. https://doi.org/10.1029/1999pa000435
- Jyothibabu, R., Arunpandi, N., Jagadeesan, L., Karnan, C., Lallu, K. R., & Vinayachandran, P. N. (2018). Response of phytoplankton to heavy cloud cover and turbidity in the northern Bay of Bengal. Scientific Reports, 8(1), 1–15. https://doi.org/10.1038/s41598-018-29586-1
- Katzenberger, A., Schewe, J., Pongratz, J., & Levermann, A. (2021). Robust increase of Indian monsoon rainfall and its variability under future warming in CMIP6 models. Earth System Dynamics, 12(2), 367–386. https://doi.org/10.5194/esd-12-367-2021
- Kroon, D., Steens, T., & Troelstra, S. R. (1991). Onset of monsoonal related upwelling in the western Arabian Sea as revealed by planktonic foraminifers. In Proc., Scientific Results, ODP, Leg (Vol. 117, pp. 257–263). Oman Margin/Neogene Package. https://doi.org/10.2973/odp.proc.sr.117.126.1991
- Kuechler, R. R., Dupont, L. M., & Schefuß, E. (2018). Hybrid insolation forcing of Pliocene monsoon dynamics in West Africa. Climate of the Past, 14(1), 73–84. https://doi.org/10.5194/cp-14-73-2018
- Kuehl, S. A., Hariu, T. M., & Moore, W. S. (1989). Shelf sedimentation off the Ganges-Brahmaputra river system: Evidence for sediment bypassing to the Bengal fan. *Geology*, 17(12), 1132–1135. https://doi.org/10.1130/0091-7613(1989)017<1132:ssotgb>2.3.co;2
- Kylander, M. E., Ampel, L., Wohlfarth, B., & Veres, D. (2011). High-resolution X-ray fluorescence core scanning analysis of Les Echets (France) sedimentary sequence: New insights from chemical proxies. *Journal of Quaternary Science*, 26(1), 109–117. https://doi.org/10.1002/jqs.1438
- Laskar, J. (2004). Long-term solution for the insolation quantities of the Earth. *Proceedings of the International Astronomical Union*, 2(14), 465. https://doi.org/10.1017/51743921307011404
- Li, J., Li, M., Wang, C., Zheng, Q., Xu, Y., Zhang, T., & Xie, L. (2023). Multiple mechanisms for chlorophyll a concentration variations in coastal upwelling regions: A case study east of Hainan Island in the South China sea. *Ocean Science*, 19(2), 469–484. https://doi.org/10.5194/os-19-469-2023
- Li, M., Hinnov, L., & Kump, L. (2019). Acycle: Time-series analysis software for paleoclimate research and education. *Computers & Geosciences*, 127(September 2018), 12–22. https://doi.org/10.1016/j.cageo.2019.02.011
- Liess, A., Faithfull, C., Reichstein, B., Guo, J., Pete, R., et al. (2015). Terrestrial runoff may reduce microbenthic net community productivity by increasing turbidity: A mediterranean coastal lagoon mesocosm experiment terrestrial runoff may reduce microbenthic net community productivity by increasing turbidity: A mediterran. March. *Hydrobiologia*, 753(1), 205–218. https://doi.org/10.1007/s10750-015-2207-3
- Lisiecki, L. E., & Raymo, M. E. (2005). A Pliocene-Pleistocene stack of 57 globally distributed benthic δ18O records. Paleoceanography, 20(1), 1–17. https://doi.org/10.1029/2004PA001071
- Liu, Z., Cleaveland, L. C., & Herbert, T. D. (2008). Early onset and origin of 100-kyr cycles in Pleistocene tropical SST records. Earth and Planetary Science Letters, 265(3–4), 703–715. https://doi.org/10.1016/j.epsl.2007.11.016
- Löwemark, L., Bloemsma, M., Croudace, I., Daly, J. S., Edwards, R. J., Francus, P., et al. (2019). Practical guidelines and recent advances in the Itrax XRF core-scanning procedure. *Quaternary International*, 514(February 2018), 16–29. https://doi.org/10.1016/j.quaint.2018.10.044
- Martínez-Botí, M. A., Foster, G. L., Chalk, T. B., Rohling, E. J., Sexton, P. F., Lunt, D. J., et al. (2015). Plio-Pleistocene climate sensitivity evaluated using high-resolution CO2 records. *Nature*, 518(7537), 49–54. https://doi.org/10.1038/nature14145
- Martínez-García, A., Rosell-Melé, A., McClymont, E. L., Rainer, G., & Haug, G. H. (2010). Subpolar link to the emergence of the modern equatorial Pacific cold Tongue. *Science*, 328(5985), 1550–1553. https://doi.org/10.1126/science.1184480
- McClymont, E. L., Ho, S.-L., Ford, H. L., Bailey, I., Berke, M. A., Bolton, C. T., et al. (2023). Climate evolution through the onset and intensification of northern hemisphere glaciation. *Reviews of Geophysics*, 61(3). https://doi.org/10.1029/2022rg000793
- Menon, A., Levermann, A., Schewe, J., Lehmann, J., & Frieler, K. (2013). Consistent increase in Indian monsoon rainfall and its variability across CMIP-5 models. *Earth System Dynamics*, 4(2), 287–300. https://doi.org/10.5194/esd-4-287-2013
- Milliman, J. D., & Meade, R. H. (1983). World-wide delivery of river sediment to the oceans. The Journal of Geology, 91(1), 1–21. https://doi.org/ 10.1086/628741
- Naidu, P. D., Ganeshram, R., Bollasina, M. A., Panmei, C., Nürnberg, D., & Donges, J. F. (2020). Coherent response of the Indian monsoon rainfall to Atlantic multi-decadal variability over the last 2000 years. *Scientific Reports*, 10(1), 1–11. https://doi.org/10.1038/s41598-020-58265
- Nilsson-Kerr, K., Anand, P., Sexton, P. F., Leng, M. J., & Naidu, P. D. (2022). Indian Summer Monsoon variability 140–70 thousand years ago based on multi-proxy records from the Bay of Bengal. *Quaternary Science Reviews*, 279(February), 107403. https://doi.org/10.1016/j.quascirev.2022.107403
- Paillard, D., Labeyrie, L., & Yiou, P. (1996). Macintosh Program performs time-series analysis. *Eos, Transactions American Geophysical Union*, 77(39), 379. https://doi.org/10.1029/96eo00259
- Phillips, S. C., Johnson, J. E., Giosan, L., & Rose, K. (2014). Monsoon-influenced variation in productivity and lithogenic sediment flux since 110ka in the offshore Mahanadi Basin, northern Bay of Bengal. Marine and Petroleum Geology, 58(PA), 502–525. https://doi.org/10.1016/j. marpetgeo.2014.05.007
- Piva, A., Asioli, A., Schneider, R. R., Trincardi, F., Andersen, N., Colmenero-Hidalgo, E., et al. (2008). Climatic cycles as expressed in sediments of the PROMESSI borehole PRAD1-2, central Adriatic, for the last 370 ka: 1. Integrated stratigraphy. *Geochemistry, Geophysics, Geosystems*, 9(1), Q01R01. https://doi.org/10.1029/2007GC001713
- Pörtner, H.-O., Roberts, D. C., Masson-Delmotte, V., Zhai, P., Tignor, M., Poloczanska, E., & Weyer, N. M. (2019). The ocean and cryosphere in a changing climate. In *IPCC special report on the ocean and cryosphere in a changing climate* (Vol. 1155). Cambridge University Press.
- Prasanna Kumar, S., Muraleedharan, P. M., Prasad, T. G., Gauns, M., Ramaiah, N., de Souza, S. N., et al. (2002). Why is the Bay of Bengal less productive during summer monsoon compared to the Arabian Sea? *Geophysical Research Letters*, 29(24), 88-1–88–4. https://doi.org/10.1029/2002GL016013
- Prasanna Kumar, S., Narvekar, J., Nuncio, M., Kumar, A., Ramaiah, N., Sardesai, S., et al. (2010). Is the biological productivity in the Bay of Bengal light limited? *Current Science*, 98(10), 1331–1339.
- Prell, W. L., & Kutzbach, J. E. (1992). Sensitivity of the Indian monsoon to forcing parameters and implications for its evolution. *Nature*, 360(6405), 647–652. https://doi.org/10.1038/360647a0
- Prescott, C. L. L., Haywood, A. M. M., Dolan, A. M. M., Hunter, S. J. J., & Tindall, J. C. C. (2019). Indian monsoon variability in response to orbital forcing during the late Pliocene. *Global and Planetary Change*, 173(April 2018), 33–46. https://doi.org/10.1016/j.gloplacha.2018. 12.002
- Raj, J., Bangalath, H. K., & Stenchikov, G. (2019). West African monsoon: Current state and future projections in a high-resolution AGCM. Climate Dynamics, 52(11), 6441–6461. https://doi.org/10.1007/s00382-018-4522-7

BOKHARI-FRIBERG ET AL. 17 of 18

- Raymo, M. (1994). The initiation of northern hemisphere glaciation. *Annual Review of Earth and Planetary Sciences*, 22(1), 353–383. https://doi.org/10.1146/annurey.earth.22.1.353
- Rayner, N. A., Parker, D. E., Horton, E. B., Folland, C. K., Alexander, L. V., Rowell, D. P., et al. (2003). Global analyses of sea surface temperature, sea ice, and night marine air temperature since the late nineteenth century. *Journal of Geophysical Research*, 108(14), 4407. https://doi.org/10.1029/2002jd002670
- Robinson, M. M., & Dowsett, H. J. (2023). Pliocene planktic foraminiferal census data from the northeast Indian Ocean and Southeast Virginia. *U. S. Geological Survey*. https://doi.org/10.5066/P9PZJMDM
- Rothwell, R. G., & Rack. (2006). New techniques in sediment core analysis: An introduction (Vol. 267, pp. 1–29). Geological Society Special Publication. https://doi.org/10.1144/GSL.SP.2006.267.01.01
- Rothwell, R. G., & Croudace, I. (2015). Twenty years of XRF core scanning marine sediments: What do geochemical proxies tell us? In *Micro-XRF Studies of Sediment Cores* (pp. 25–102). Springer.
- Ruddiman, W. F., Raymo, M., & McIntyre, A. (1986). Matuyama 41,000-year cycles: North Atlantic Ocean and northern hemisphere ice sheets. Earth and Planetary Science Letters, 80(1–2), 117–129. https://doi.org/10.1016/0012-821X(86)90024-5
- Sancetta, C., & Calvert, S. E. (1988). The annual cycle of sedimentation in Saanich inlet, British Columbia: Implications for the interpretation of diatom fossil assemblages. *Deep-Sea Research, Part A: Oceanographic Research Papers*, 35(1), 71–90. https://doi.org/10.1016/0198-0149 (88)90058-1
- Sarma, V. V. S. S., Chopra, M., Rao, D. N., Priya, M. M. R., Rajula, G. R., Lakshmi, D. S. R., & Rao, V. D. (2020). Role of eddies on controlling total and size-fractionated primary production in the Bay of Bengal. *Continental Shelf Research*, 204(April), 104186. https://doi.org/10.1016/j.csr.2020.104186
- Schrader, H., & Gersonde, R. (1978). Diatoms and silicoflagellates. In Zachariasse Etb Al. Microplaeontological Counting Methods and Techniques-an Excercise on an Eight Metres Section of the Lower Pliocene of Capo Rossello. Sicily (Vol. 17, pp. 129–176). Utrecht Micropal. Bull
- Seki, A., Tada, R., Kurokawa, S., & Murayama, M. (2019). High-resolution Quaternary record of marine organic carbon content in the hemipelagic sediments of the Japan Sea from bromine counts measured by XRF core scanner. *Progress in Earth and Planetary Science*, 6(1), 1–12. https://doi.org/10.1186/s40645-018-0244-z
- Shackleton, N. J., Backman, J., Zimmerman, H., Kent, D. V., Hall, M. A., Roberts, D. G., et al. (1984). Oxygen isotope calibration of the onset of ice-rafting and history of glaciation in the North Atlantic region. *Nature*, 307(February), 620–623. https://doi.org/10.1038/307620a0
- Shackleton, N. J., & Opdyke, N. D. (1973). Oxygen isotope and palaeomagnetic stratigraphy of Equatorial Pacific core V28-238: Oxygen isotope temperatures and ice volumes on a 105 year and 106 year scale. *Quaternary Research*, 3(1), 39–55. https://doi.org/10.1016/0033-5894(73) 90052-5
- Shrivastav, A., Singh, A. K., Sinha, D. K., Kaushik, T., Singh, V. P., & Mallick, K. (2016). Significance of Globigerina bulloides D'orbigny: A foraminiferal proxy for Palaeomonsoon and past upwelling records. *Journal of Climate Change*, 2(2), 99–110. https://doi.org/10.3233/jcc-160021
- Singh, R. K. (2021). Acc: Paleoceanographic turnovers during the Plio-pleistocene in the southeastern Indian ocean: Linkages with northern hemisphere glaciation and Indian monsoon variability. *Palaeogeography, Palaeoclimatology, Palaeoecology*, 104540. https://doi.org/10.1016/j.palaeo.2021.110374
- Subramanian, V. (1993). Sediment load of Indian rivers. Current Science, 64(11-12), 928-930.
- Tapia, R., Ling Ho, S., Nuñez-Ricardo, S., Marchant, M., Lamy, F., & Hebbeln, D. (2021). Increased marine productivity in the southern Humboldt current system during MIS 2 4 and 10 11. *Paleoceanography and Paleoclimatology*, 36, 1–18. https://doi.org/10.1029/2020PA004066
- Thomson, J. R., Holden, P. B., Anand, P., Edwards, N. R., Porchier, C. A., & Harris, N. B. W. (2021). Tectonic and climatic drivers of Asian monsoon evolution. *Nature Communications*, 12(1), 4022. https://doi.org/10.1038/s41467-021-24244-z
- Tiedemann, R., Sarnthein, M., & Shackleton, N. (1994). Astronomic timescale for the Pliocene Atlantic d18O and dust flux records of Ocea Drilling Program site 659. *Paleoceanography*, 9(4), 619–638. https://doi.org/10.1029/94pa00208
- Tripathi, S., Tiwari, M., & Behera, P. (2023). Prolonged South Asian monsoon variability and weakened denitrification during mid-pleistocene transition. *Palaeogeography, Palaeoclimatology, Palaeoecology*, 624(May), 111637. https://doi.org/10.1016/j.palaeo.2023.111637
- Turner, A. G., & Annamalai, H. (2012). Climate change and the South Asian summer monsoon. *Nature Climate Change*, 2(8), 587–595. https://doi.org/10.1038/nclimate1495
- Wang, B., Jin, C., & Liu, J. (2020). Understanding future change of global monsoons projected by CMIP6 models. *Journal of Climate*, 33(15), 6471–6489. https://doi.org/10.1175/JCLI-D-19-0993.1
- Wei, G., Li, X. H., Liu, Y., Shao, L., & Liang, X. (2006). Geochemical record of chemical weathering and monsoon climate change since the early Miocene in the South China Sea. *Paleoceanography*, 21(4), 1–11. https://doi.org/10.1029/2006PA001300
- Werner, D., & Roth, R. (1977). Productivity of diatoms in Culture and in marine habitats. *Marine Research in Indonesia*, 20(1966), 99–113. https://doi.org/10.14203/mri.v20i0.385
- Westerhold, T., Marwan, N., Drury, A. J., Liebrand, D., Agnini, C., Anagnostou, E., et al. (2020). An astronomically dated record of Earth's climate and its predictability over the last 66 million years. *Science*, 369(6509), 1383–1388. https://doi.org/10.1126/SCIENCE.ABA6853
- Wilson, D. J., Bertram, R. A., Needham, E. F., van de Flierdt, T., Welsh, K. J., McKay, R. M., et al. (2018). Ice loss from the East Antarctic ice sheet during late pleistocene interglacials. *Nature*, 561(7723), 383–386. https://doi.org/10.1038/s41586-018-0501-8
- Wunsch, C. (2004). Quantitative estimate of the Milankovitch-forced contribution to observed Quaternary climate change. *Quaternary Science Reviews*, 23(9–10), 1001–1012. https://doi.org/10.1016/j.quascirev.2004.02.014
- Yamamoto, M., Clemens, S. C., Seki, O., Tsuchiya, Y., Huang, Y., O'ishi, R., & Abe-Ouchi, A. (2022). Increased interglacial atmospheric CO2 levels followed the mid-Pleistocene Transition. *Nature Geoscience*, 15(4), 307–313. https://doi.org/10.1038/s41561-022-00918-1
- Zahn, R., Winn, K., & Sarnthein, M. (1986). Benthic foraminiferal d13C and accumulation rates of organic carbon: Uvigerina peregrina group and Cibicidoides wuellestorfi. *Paleoceanography*, 1(1), 27–42. https://doi.org/10.1029/pa001i001p00027
- Zhang, Z., Licht, A., De Vleeschouwer, D., Wang, Z., Li, Y., Kemp, D. B., et al. (2022). East Asian monsoonal climate sensitivity changed in the late Pliocene in response to northern hemisphere glaciations. *Geophysical Research Letters*, 49(23), 0–11. https://doi.org/10.1029/2022GL101280
- Zhou, W., Kong, X., Paterson, G. A., Sun, Y., Wu, Y., Ao, H., et al. (2023). Eccentricity-paced geomagnetic field and monsoon rainfall variations over the last 870 kyr. *Proceedings of the National Academy of Sciences*, 120(17), 2017. https://doi.org/10.1073/pnas
- Ziegler, M., Jilbert, T., De Lange, G. J., Lourens, L. J., & Reichart, G. J. (2008). Bromine counts from XRF scanning as an estimate of the marine organic carbon content of sediment cores. Geochemistry, Geophysics, Geosystems, 9(5), 1–6. https://doi.org/10.1029/2007GC001932

BOKHARI-FRIBERG ET AL. 18 of 18